A modular CRISPR screen identifies individual and combination pathways contributing to HIV-1 latency

Emily Hsieh[1], Derek H Janssens[2], Patrick J Paddison[3], Edward P Browne[4], Steve Henikoff[2,5], Molly OhAinle[3,6], Michael Emerman[2,3*]

[1]Molecular and Cellular Biology Graduate Program, University of Washington, Seattle, WA, USA
[2]Division of Basic Sciences, Fred Hutchinson Cancer Center, Seattle, WA, USA
[3]Division of Human Biology, Fred Hutchinson Cancer Center, Seattle, WA, USA
[4]Division of Infectious Diseases, Department of Medicine, University of North Carolina at Chapel Hill, Chapel Hill, NC, USA
[5]Howard Hughes Medical Institute, Chevy Chase, MD, USA
[6]current address: Division of Immunology and Molecular Medicine, Department of Molecular and Cell Biology, University of California, Berkeley, CA, USA

*Corresponding author: Michael Emerman, memerman@fredhutch.org

Abstract

Transcriptional silencing of latent HIV-1 proviruses entails complex and overlapping mechanisms that pose a major barrier to *in vivo* elimination of HIV-1. We developed a new latency CRISPR screening strategy, called Latency HIV-CRISPR, which uses the packaging of guideRNA-encoding lentiviral vector genomes into the supernatant of budding virions as a direct readout of factors involved in the maintenance of HIV-1 latency. We developed a custom guideRNA library targeting epigenetic regulatory genes and paired the screen with and without a latency reversal agent – AZD5582, an activator of the non-canonical NFκB pathway – to examine a combination of mechanisms controlling HIV-1 latency. A component of the Nucleosome Acetyltransferase of H4 histone acetylation (NuA4 HAT) complex, ING3, acts in concert with AZD5582 to activate proviruses in J-Lat cell lines and in a primary CD4+ T cell model of HIV-1 latency. We found that the knockout of *ING3* reduces acetylation of the H4 histone tail and BRD4 occupancy on the HIV-1 LTR, and only in the combination of *ING3* knockout with the activation of non-canonical NFκB via AZD5582 is there dramatic increase in initiation and elongation of RNA Polymerase II on the HIV-1 provirus in a manner that is nearly unique among all cellular promoters.

42 **Introduction**
43
44 Effective antiretroviral therapy (ART) can drive HIV-1 viral loads to undetectable
45 levels [1]. However, ART does not eliminate the virus from people living with HIV-1.
46 Upon interruption of ART, there is a rapid rebound of virus replication from a long-lived
47 latent reservoir primarily found in memory CD4+ T cells among other cell types [2]. This
48 latent reservoir of replication-competent HIV-1 proviruses is a significant obstacle to the
49 complete clearance of HIV-1 [3], and purging or managing this latent reservoir is
50 essential to achieve a functional cure.
51 The latent HIV-1 reservoir is often transcriptionally silent but can produce
52 infectious virus upon T-cell activation [4]. The transcriptional silencing of the provirus in
53 HIV-1 latency is dependent on integration site [5, 6] and a breadth of host factors that
54 limit transcriptional initiation and elongation of the HIV-1 proviral genome (reviewed in
55 [7]). Small molecule inhibitors or activators, known as latency reversal agents (LRAs),
56 have been shown to activate HIV-1 viral transcription in cell line models of HIV-1 latency
57 [8] and in primary cell cultures derived from people living with HIV-1 [9, 10]. AZD5582 is
58 a second mitochondria-derived activator of caspases (SMAC) mimetic that is an
59 example of an LRA that provides some specificity for latency reversal by activating the
60 non-canonical NFκB pathway [11]. Many LRAs have shown success at reactivating
61 latent HIV-1 in HIV-1 latency models, but even the most well-established LRAs have
62 modest or no effect in clinical trials on their own [12]. This highlights the complexity of
63 mechanisms involved in maintaining the HIV-1 latent state, and the need to identify
64 novel epigenetic factors and transcriptional mechanisms controlling HIV-1 latency.

65 Studies on the functional role of host epigenetic regulation of HIV-1 transcription
66 (reviewed in [7, 13, 14]) has resulted in the identification of some specific host
67 epigenetic regulatory genes that are involved in maintaining HIV-1 latency. For
68 example, KAT5 of the Nucleosome Acetyltransferase of H4 histone acetylation (NuA4
69 HAT) complex deposits a uniquely high profile of acetylated lysine residues on the H4
70 histone tail (H4Ac) found at the HIV-1 provirus LTR [9]. This results in the recruitment of
71 the long isoform of the *Bromodomain Containing 4* (*BRD4*) gene [9, 15, 16].
72 Additionally, the long BRD4 isoform in *in vitro* experiments serves as a competitor for
73 positive transcription elongation factor b (P-TEFb) binding to the HIV-1 transactivator,
74 Tat [16]. *BRD4* also encodes a short isoform that recruits the repressive BAF complex
75 to the HIV-1 provirus [17]. Another set of genes implicated in HIV-1 latency through
76 repression of HIV-1 transcription, encode components of the Polycomb Repressive
77 Complex 2 (PRC2) [10, 18, 19]. PRC2 catalyzes the methylation of histone H3 Lysine
78 27 to maintain transcriptional repression of genes, including throughout development.
79 The use of genetic screens has been effective in revealing pathways involved in
80 HIV-1 latency in a single-gene manner [10, 20-27]. Here, we sought to create a novel
81 CRISPR-based screening platform with the capacity to allow for rapid, parallel
82 assessment of multiple pathways that contribute to the maintenance of HIV-1 latency
83 both with and without the presence of additional LRAs. We reasoned that by combining
84 LRAs of one mechanism with a CRISPR screen that targets a different mechanism, we
85 could uncover latency reversal pathways with increased potency and specificity for the
86 HIV-1 LTR. We established a novel HIV-based latency CRISPR screening strategy that

87 uses J-Lat cells [28, 29] in combination with our recently developed HIV-CRISPR
88 screening methodology [30] to use reactivation of the latent provirus as the reporter for
89 the screen. To identify epigenetic pathways that act with and without LRAs to activate
90 latent proviruses, we generated a custom CRISPR library targeting epigenetic
91 regulatory genes and performed the screen in the absence and presence of a low-
92 activating dose of AZD5582. In the absence of AZD5582, we found *CUL3*, a scaffold for
93 an E3 ubiquitin ligase, as a novel HIV-1 latency maintenance and establishment factor
94 in both J-Lat cells and a primary CD4+ T cell model of HIV-1 latency. Moreover, we
95 identified the NuA4 HAT complex to be of importance to HIV-1 latency, specifically two
96 complex subunit members – ACTL6A and ING3. In particular, *Inhibitor of Growth Family*
97 *Member (ING3)* knockout combined with AZD5582 treatment resulted in enhanced viral
98 reactivation in the J-Lat cells and a primary CD4+ T cell model of HIV-1 latency. By
99 using automated CUT&Tag to investigate genome-wide chromatin occupancy [31], we
100 found that *ING3* knockout alone and in combination with AZD5582 treatment results in
101 the reduction of H4Ac and BRD4 levels at the HIV-1 LTR. However, only in the
102 presence of AZD5582 in the *ING3* knockout cells, do we see a substantial increase in
103 RNA Polymerase II Serine 5 phosphorylation (RNA-Pol2-S5p) occupancy at the LTR
104 and this dramatic increase is nearly unique among all promoters in the human genome.
105 Simultaneously, the combination of *ING3* knockout and AZD5582 treatment results in
106 increases in RNA-Pol2-S5p and RNA-Pol2-S2p within the body of the provirus, which
107 indicates increased transcription initiation and elongation and correlates with the

108 increase of viral reactivation. Our novel HIV-CRISPR screening approach provides an
109 avenue to explore factors that act in combination to promote HIV-1 latency.
110
111 **Results**
112
113 Latency HIV-CRISPR identifies novel epigenetic factors involved in maintaining HIV-1
114 latency
115 Our aim was to establish a high throughput CRISPR-Cas9 knockout strategy for
116 investigating the complexities of epigenetic regulation of HIV-1 latency. We leveraged a
117 previously described HIV-CRISPR vector [30] which is a lentiviral based vector with two
118 intact LTRs, a packaging signal, Cas9, and a library of single guide RNAs (sgRNAs).
119 The unique feature of the HIV-CRISPR vector is that in the presence of replication-
120 competent HIV-1, the genome of the HIV-CRISPR vector is transcribed into RNA and
121 packaged *in trans* into HIV-1 virions. We reasoned that in J-Lat cells, an *in vitro* T-
122 lymphocyte HIV-1 latency model which harbors a near full-length HIV-1 provirus, any
123 sgRNAs encoded in HIV-CRISPR genomes that target candidate HIV-1 latency genes
124 will be packaged into the reactivated virus particle, secreted, and enriched in the viral
125 supernatant (**Figure 1A**). Consequently, the RNA of the viral supernatant from the HIV-
126 CRISPR latency screen can undergo next-generation sequencing to determine sgRNAs
127 that are enriched in the viral particles and thereby identify candidate genes involved in
128 HIV-1 latency maintenance. This results in a direct readout for the gene knockout which
129 incorporates functional, reactivation activity.
130 To specifically investigate host epigenetic regulators involved in the maintenance
131 of HIV-1 latency, we generated a custom human epigenome specific sgRNA CRISPR

132 library (HuEpi). This library contains sgRNAs targeting epigenome factors such as
133 histones, histone binders (e.g., histone readers and chaperones), histone modifiers
134 (e.g., histone writers and erasers), and general chromatin associated factors (e.g., RNA
135 and DNA modifiers) (**Figure 1B, C**). Most of the genes targeted in this library are
136 derived from the EpiFactor database [32]. To this set we also added histones and other
137 hand-selected gene regulatory complexes. The total library contains 5,309 sgRNAs
138 targeting 841 genes (6 sgRNAs per gene with a few exceptions) and 252 non-targeting
139 controls (NTCs) [33] (**Supplemental Table 1**). The small size of the library improves the
140 likelihood of high coverage of all the sgRNAs throughout the CRISPR screening
141 process relative to a whole-genome screen.

142 The sgRNA sequences from the HuEpi library were cloned in bulk into the HIV-
143 CRISPR vector and the lentiviral library was subsequently transduced into J-Lat cells at
144 a low MOI (MOI = 0.4) (**Figure 1D-1**). We transduced two independent J-Lat cell clones,
145 the J-Lat 10.6 [28] and J-Lat 5A8 [29] cells, which each have different proviral
146 integration sites and the latter of which responds to LRAs more similarly to primary
147 CD4+ T cell HIV-1 latency models compared to other cell line models [34]. Transduced
148 cells were then subjected to 10-14 days of puromycin selection after which the cells and
149 viral supernatant were harvested and processed by next-generation sequencing of the
150 sgRNAs to identify the candidate HIV-latency genes (**Figure 1D-3**). Genomic DNA was
151 extracted from the cell pellet to determine the baseline representation of each sgRNA in
152 the transduced sgRNA library. Viral RNA was extracted from the concentrated viral
153 supernatant to identify the sgRNA population that facilitated latent HIV-1 provirus

154 transcription reactivation (**Figure 1D-4**). Using the MAGeCK pipeline [35], we identified
155 candidate HIV-1 latency maintenance factors by selecting genes in which the sgRNA
156 counts of the viral RNA were enriched compared to the sgRNA counts in the genomic
157 DNA. Genes with an increased sgRNA count in the viral RNA, which equates to an
158 increase in the fold change, are predicted to play a role in maintaining HIV-1 latency.

159 Overall, the Latency HIV-CRISPR screen results for both J-Lat 10.6 and J-Lat
160 5A8 cell lines demonstrated a significant enrichment in specific sgRNAs compared to
161 the NTCs. We compared the distribution of the log fold change (LFC) of NTCs against
162 the gene targeting sgRNAs. While the LFC of most gene targeting sgRNAs clustered
163 around the median LFC of the NTCs, we observed that a subset of the gene targeting
164 sgRNAs were significantly enriched compared to the NTC population. These sgRNAs
165 are the sgRNAs of interest that target potential HIV-1 latency maintenance factor genes
166 (**Figure 2A**).

167 To determine top candidate genes from the Latency HIV-CRISPR screen, we
168 ranked the genes by MAGeCK gene score. For both J-Lat cell lines, we observe that
169 there are many genes that are significantly enriched compared to the NTCs. We
170 identified eight previously unreported epigenetic HIV-1 latency maintenance genes,
171 defined by a false discovery rate (FDR) less than 10% in both J-Lat 10.6 and J-Lat 5A8
172 cell lines, as our top hits (**Figure 3A**). BRD4 and KAT5 are two host factors previously
173 reported to silence HIV-1 transcription ([16, 17, 36] and [9], respectively), and in our
174 screen, the sgRNAs targeting *BRD4* and *KAT5* are significantly enriched compared to
175 the sgRNAs targeting NTCs in both J-Lat cell lines (**Figure 2B; Supplemental Table 2**).

176 In addition to individual genes, the Latency HIV-CRISPR screen also identified genes
177 encoding subunits of protein complexes important to HIV-1 latency. PRC2 has also
178 been previously reported to silence HIV-1 transcription [8, 10] and members of the
179 complex including *EZH2*, the catalytic component, and *SUZ12* and *EED* showed a trend
180 of enrichment in our screen (**Figure 2B; Supplemental Table 2**). Thus, our Latency
181 HIV-CRISPR screen system identifies bona fide HIV-1 latency maintenance factors.
182

183 <u>The Latency HIV-CRISPR screen identifies multiple members of the NuA4 complex and</u>
184 <u>CUL3</u>

185 To identify the top candidate HIV-1 latency genes, we integrated the guideRNA
186 data to a gene level using MAGeCK analysis [35] (**Figure 3A; Supplemental Table 3**).
187 As we were primarily interested in hits that are independent of integration site, we
188 considered the top gene hits as those that that have an FDR < 10% and also are shared
189 between both J-Lat 10.6 and J-Lat 5A8 cell lines (**Figure 3B**, middle of Venn diagram).
190 We observed that multiple members of the Nucleosome Acetyltransferase of H4 (NuA4)
191 complex scored highly in the screen (**Figure 3A**). The NuA4 complex is highly
192 conserved in eukaryotes [37] and acetylates histone H4 [38] and has been implicated in
193 many genomic processes including DNA damage repair and transcription [39]. Many
194 proteins that are part of the NuA4 complex also overlap with the SNF2-Related CBP
195 Activator Protein (SRCAP) complex which exchanges the H2A of the canonical
196 nucleosome with the H2A.Z variant [40-42]. A gene ontology (GO) enrichment analysis
197 [43] of the top gene hits (FDR <10% for each J-Lat cell line) demonstrated that the

198 SRCAP-associated chromatin remodeling complex is highly enriched in both J-Lat cell
199 lines (**Figure 3C**) and is different from the overall GO distribution of the total HuEpi
200 library (**Figure 1C**), demonstrating the screen specifically enriched for specific
201 pathways. Based on the MAGeCK gene scores, six of the seven genes (*BRD8*, *DMAP1*,
202 *RUVBL1*, *RUVBL2*, *ACTL6A*, *VPS72*, and *YEATS4*) that encode proteins overlapping
203 between the NuA4 HAT and SRCAP complexes scored higher than the median
204 MAGeCK score for the NTCs (**Figure 3D**). The only exception is *RUVBL1* in the J-Lat
205 10.6 screen, which scored below the NTC median MAGeCK score (RUVBL1 = 0.318 vs
206 NTC median = 0.518). Additionally, most genes unique to each complex also had
207 MAGeCK scores above the NTC median in both cell lines. Genes unique to the NuA4
208 HAT complex included *TRRAP*, *EP400*, *EPC2*, *KAT5*, *ING3*, *MORF4L1*, *MORF4L2*,
209 *MEAF6*, and *MBTD1* and genes unique to the SRCAP complex included *SRCAP* and
210 *ZNHIT1* (**Figure 3D**). This analysis suggests that the Latency HIV-CRISPR screen
211 strategy can extend beyond identification of single genes of interest to groups of genes
212 encoding complexes of relevance, which can further shed light on the mechanisms
213 involved in maintaining HIV-1 latency.

214 To validate the top screen hits, we generated four individual J-Lat 10.6 and 5A8
215 knockout cell lines for each gene (two sgRNAs per gene). To avoid clone-to-clone
216 differences, each of these knockout cell lines represents a pool of knockout cells rather
217 than clones. As positive controls, we used two sgRNAs targeting *NFκBIA*, an inhibitor
218 for NFκB, and a gene that was not included in the HuEpi library. Upon knockout of
219 *NFκBIA* in the J-Lat cells, we expect an increase in HIV-1 transcriptional activity, which

220 leads to virus production. As negative controls, we used two NTC sgRNAs that do not
221 target human loci. To assess latency reversal in the J-Lat cells, we measured HIV-1
222 reverse transcriptase activity in the supernatant, which is a readout after the viral
223 transcription, translation, and budding steps have occurred. Because the transduced
224 cells were assayed as a pool of gene knockouts, we simultaneously measured CRISPR
225 editing efficiency in bulk using the program Inference of CRISPR Edits (ICE) [44]. The
226 knockout efficiency for the heterogenous cell lines we generated varied between 32% to
227 83% (**Figure 4A**). A recent study demonstrated that a median knockout of 35% was
228 less efficient, but still had a meaningful effect [45].

229 Compared to the cell lines transduced with NTC sgRNAs, we found that
230 individually knocking out all eight novel candidate gene hits resulted in significant
231 latency reversal in at least one of the J-Lat cell lines we tested (**Figure 4A**). In fact,
232 some of the reverse transcriptase measurements from the gene knockout cell lines are
233 comparable to the positive control knockout of *NFκBIA*. In addition, we confirmed that
234 knockout of a top scoring gene hit in our screen, *KAT5*, a previously reported HIV-1
235 latency maintenance factor [9], results in viral reactivation in both J-Lat cell lines (**Figure**
236 **4A**). Moreover, genes encoding protein components of the NuA4 HAT and SRCAP
237 complexes described above, *ACTL6A*, *DMAP1*, *VPS72*, and *YEATS4* also all validated
238 as latency maintenance factors in J-Lat cells (**Figure 4A**). *ACTL6A* knockout results in a
239 particularly high level of HIV-1 reactivation, which may be a result of *ACTL6A* encoding
240 a protein that is a subunit of both NuA4 HAT and SRCAP complexes (**Figure 3D**). Other
241 genes validated in this functional investigation include *DMAP1* which encodes a protein

242 that forms a complex with DNMT1 to mediate transcriptional repression [46] and has
243 been described to play a role in HIV-1 latency in some studies [14] and *TAF5* which
244 functions in scaffold formation and is a critical subunit of the general transcription factor
245 TFIID.

246 As *CUL3* was the top gene hit in our Latency HIV-CRISPR screen in both J-Lat
247 10.6 and J-Lat 5A8 cell lines and validated as a latency maintenance factor in J-Lat
248 cells, we further characterized *CUL3* in the context of a primary CD4+ T cell HIV-1
249 latency model system. CUL3 is part of the cullin family and serves as the scaffold for
250 Cullin-RING E3 ligase complexes, which ubiquitinate proteins [47]. For our primary cell
251 HIV-1 latency model system, we used a dual HIV-1 reporter virus (pNL4-3-Δ6-dreGFP-
252 CD90) that is derived from previously established systems [48, 49]. Here, the reporter
253 virus has been modified to encode a destabilized eGFP gene and a mouse Thy1.2
254 (CD90.2) gene, which are separated by an IRES and both reporters are under control of
255 the HIV-1 LTR [50]. As the mouse Thy1.2 reporter has a long half-life and is slow to turn
256 over, it serves as a marker to determine the cells that have been infected by the
257 reporter virus (Thy1.2+). Amongst the infected cells (Thy1.2+), the eGFP reporter,
258 which has a short half-life, serves as a marker to determine the cells that are actively
259 transcribing or actively infected (Thy1.2+, GFP+) versus minimally transcribing or
260 latently infected (Thy1.2+, GFP-). We knocked out *CUL3* in the primary CD4+ T cell
261 HIV-1 latency model using Cas9-gRNA ribonucleoproteins (RNPs) including 3 different
262 sgRNAs. As a negative control, the *AAVS1* gene is targeted for knockout, which is in a

263 “safe harbor” locus in which disruption of this gene does not have adverse effects on the
264 cell [51].

265 We expected that if CUL3 plays a role in HIV-1 latency establishment, there will
266 be a higher reactivated population in the *CUL3* knockout cells compared to the negative
267 control (*AAVS1*) knockout cells. We acquired CD4+ T cells from four healthy donors and
268 infected the cells with the dual reporter virus. Indeed, upon performing the described
269 CRISPR/Cas9-mediated knockout and measuring the functional output of the reporter
270 virus, we observed that *CUL3* knockout in all four donors resulted in significant HIV-1
271 reactivation and subsequent decrease in the latent population compared to *AAVS1*
272 knockout (**Figure 4B; Supplemental Figure 1A**). This suggests that post-translational
273 ubiquitin modification of a substrate by CUL3 may facilitate the establishment and
274 maintenance of HIV-1 latency. Our data is consistent with previous work as CUL3 has
275 been demonstrated to negatively regulate HIV-1 transcription during productive infection
276 directly or indirectly through the NFκB pathway as NFκB/NFAT binding sites at the LTR
277 are critical for regulating viral transcription [52]. Moreover, these data demonstrate that
278 the Latency HIV-CRISPR screening strategy is effective in identifying novel epigenetic
279 HIV-1 latency maintenance genes that have been validated in multiple systems.

280

281 <u>An LRA Latency HIV-CRISPR screen reveals regulatory changes that act in</u>
282 <u>combination during reactivation of HIV-1 latency</u>

283 A critical extension of this HIV-CRISPR latency screen methodology is the ability
284 to examine other transcriptional mechanisms in conjunction with epigenetic regulatory

285 factors. Thus, to address HIV-1 latency as a state of multiple, parallel mechanisms, we
286 modified the screen by treating the pool of human epigenome knockout cells with a low-
287 activating dose of LRA. The goal was to identify instances of combinations between the
288 gene knockout and LRA resulting in a significant increase in viral reactivation (i.e. a top
289 hit in the screen). As a proof of principle, we used the recently identified LRA, AZD5582,
290 which is a SMAC mimetic and non-canonical NFκB activator [11]. We first determined
291 10 nM AZD5582 as the low-activating dose of LRA to use by performing an HIV-1 viral
292 reactivation dose curve using both J-Lat cell lines (**Supplemental Figure 2A**). The
293 same HuEpi knockout pool of cells used in the Latency HIV-CRISPR screen described
294 in **Figure 3** were in parallel treated for 24 hours with 10 nM of AZD5582 (**Figure 1D-2**).
295 This allows for the identification of epigenetic regulatory genes that upon knockout,
296 combine with the transcriptional initiation pathway targeted by AZD5582, to result in a
297 significant increase in viral reactivation.

298 The most prominent hit of the AZD5582 LRA Latency HIV-CRISPR screen in
299 both J-Lat cell lines was *Inhibitor of Growth Family Member 3* (*ING3*), a novel HIV-1
300 latency factor (**Figure 5A; Supplemental Table 4, 5**). To confirm that *ING3* was a top
301 gene hit unique to the LRA condition, we compared the LRA Latency HIV-CRISPR
302 screen results to the Latency HIV-CRISPR screen results in the absence of LRA.
303 Overall, many gene hits overlapped between the Latency HIV-CRISPR screen in the
304 presence and absence of AZD5582 (**Figure 5B**). For example, the previously identified
305 *KAT5* gene and genes that we validated in **Figure 4** including *DNMT1*, *YEATS4*, and
306 *ACTL6A* were still amongst the top gene hits, which suggests that these genes broadly

307 play a role in HIV-1 latency maintenance regardless of activation of the non-canonical
308 NFκB pathway. We verified that *ING3* was the top gene hit unique to the screen in the
309 presence of AZD5582 and sought to perform additional validation for this gene. We also
310 observed that *CUL3*, the top hit unique to the screen in the absence of AZD5582, was
311 relatively depleted in the screen conducted in the presence of AZD5582 (**Figure 5B**).
312 This suggests a potential overlap between AZD5582 non-canonical NFκB function and
313 *CUL3* function in the context of HIV-1 latency reversal.

314 To validate *ING3*, the top hit enriched in the AZD5582 LRA Latency HIV-CRISPR
315 arm of the screen, we generated *ING3* knockout cell lines in both J-Lat 10.6 and 5A8
316 cells. Simultaneously, cell lines transduced with the NTC sgRNAs were generated as a
317 negative control. The pools of knockout cells were treated with or without a low
318 reactivating dose (10 nM) of AZD5582 for 24 hours and then viral reactivation was
319 measured by HIV-1 reverse transcriptase activity. Based on screen results, we
320 hypothesized that knockout of *ING3* alone would result in some level of viral reactivation
321 compared to the transduction of NTC sgRNAs, but upon treatment with a low
322 reactivating dose of AZD5582, viral reactivation would become even more pronounced.
323 Consistent with our hypothesis, we observed that in both J-Lat cell lines, low
324 reactivating dose AZD5582 treatment of the cell lines transduced with the NTC sgRNAs
325 results in minimal viral reactivation, but treatment of the *ING3* knockout cell lines results
326 in significant, increased viral reactivation (**Figure 6A**). These results suggest a
327 mechanistic interplay between *ING3* inhibition and AZD5582 treatment during the
328 reactivation of HIV-1 transcription. Moreover, we observed a similar trend in the primary

329 CD4+ T cell HIV-1 latency model described previously. In healthy donor samples of
330 CD4+ T cells in which the latency model was established, we performed a total of four
331 independent *AAVS1* and *ING3* knockouts (three independent knockouts with one donor
332 and one knockout with a second donor), followed by 1 μM AZD5582 treatment, and
333 observed significant viral reactivation in the combination condition of *ING3* knockout and
334 AZD5582 treatment (**Figure 6B, C**). This enhancement of viral reactivation in two
335 latency models suggests that there may be interplay between the function of *ING3* and
336 the non-canonical NFκB pathway, which is targeted by AZD5582, both in cell lines and
337 in primary CD4+ T cells.

338 As AZD5582 activates the non-canonical NFκB pathway, it is possible that *ING3*
339 knockout could either enhance this activity or act through an independent pathway in
340 the context of HIV-1 viral reactivation. To distinguish between these two possibilities, we
341 measured the protein levels of NFκB2 products which includes p100, the cytoplasmic
342 NFκB2 protein, and p52, the cleaved and active subunit that translocates to the
343 nucleus. As expected, activation of the non-canonical NFκB upon AZD5582 treatment
344 results in an increase in the cleaved p52 product and a decrease in the p100 product in
345 the control (NTC) cells (**Figure 6D**). We find that p52 levels are similar in the control
346 and *ING3* knockout J-Lat cell lines (**Figure 6D**) suggesting that another pathway
347 besides the non-canonical NFκB is the main driver resulting in HIV-1 reactivation.
348 Altogether the LRA Latency HIV-CRISPR screen demonstrates the powerful potential
349 for examining multiple mechanisms simultaneously to gain a more comprehensive

350 understanding of the mechanisms underpinning HIV-1 latency and to further improve
351 existing LRAs.
352
353 The combination of ING3 knockout and AZD5582 treatment uniquely results in
354 significant increases of RNA-Pol2-S5p levels at the HIV-1 provirus
355 To better understand how AZD5582 treatment and *ING3* knockout act in
356 combination to promote reactivation of latent HIV-1 proviruses, we examined the
357 chromatin-related changes to the HIV-1 provirus by performing automated CUT&Tag
358 [31]. Specifically, we performed genome-wide profiling of the J-Lat 10.6 cell line under
359 four different conditions: (i) Transduction of NTC sgRNA with a treatment of DMSO
360 (NTC + DMSO), the negative control (ii) Transduction of NTC sgRNA with a treatment of
361 10 nM AZD5582 (NTC + AZD5582) (iii) *ING3* knockout with a treatment of DMSO (ING3
362 KO + DMSO) (iv) *ING3* knockout with a treatment of 10 nM AZD5582 (ING3 KO +
363 AZD5582).
364 ING3 is a known member of the NuA4 HAT complex, which functions to acetylate
365 the histone H4 tail [53]. BRD4 interacts with acetylated H4 [9] and both isoforms of
366 BRD4 are known to negatively regulate HIV-1 transcription [16, 17]. Therefore, our
367 hypothesis is that significant viral reactivation identified only in the combination of *ING3*
368 knockout and AZD5582 treatment would be correlated with changes in levels of H4
369 acetylation, BRD4, and active RNA polymerase at the integrated provirus. As a result,
370 we performed automated CUT&Tag using antibodies that recognized acetylated histone
371 H4 (pan-H4Ac), BRD4, RNA-Pol2-S5p, RNA-Pol2-S2p, as well as a non-specific IgG

372 negative control, at both the HIV-1 provirus genome and globally across the human
373 genome.

374 We observed no change in pan-H4Ac signal over the HIV-1 LTR upon 10 nM
375 AZD5582 treatment, but consistent with the known function of ING3, upon *ING3*
376 knockout, there was a significant decrease in pan-H4Ac signal at the HIV-1 LTR
377 (p=0.0061) (**Figure 7A, B**). Additionally, the combination of *ING3* knockout with
378 AZD5582 treatment, resulted in a significant decrease in pan-H4Ac signal at the HIV-1
379 LTR (p=0.0415). Notably, in the *ING3* knockout condition alone, we observed a
380 significant decrease in pan-H4Ac signal over both the U3 region of the HIV-1 LTR
381 (p=0.0070) as well as a significant decrease in the pan-H4Ac signal in the R and U5
382 region of the HIV-1 LTR (p=0.0126) containing the HIV-1 provirus transcription start site
383 (**Figure 7A, B**). When the *ING3* knockout is combined with AZD5582 treatment, there is
384 only a significant decrease in the R and U5 region of the HIV-1 LTR (p=0.0016). Thus,
385 *ING3* knockout appears to be the main driver of the change in pan-H4Ac levels on the
386 HIV-1 LTR in the presence and absence of AZD5582. We also find that that the
387 reduction in pan-H4Ac levels we observed on the HIV-1 LTR in the *ING3* knockout
388 condition correlate with reduced recruitment of BRD4. Indeed, as compared to NTC +
389 DMSO, AZD5582 treatment alone did not affect BRD4 levels over the HIV-1 LTR;
390 however, BRD4 levels were significantly decreased over the LTR both in the condition
391 of *ING3* knockout alone and in combination with AZD5582 treatment (p=0.0235,
392 p=0.0349, respectively) (**Figure 7C, D**). In the absence of AZD5582, the *ING3* knockout
393 results in a significant decrease in the occupancy of BRD4 only over the U3 region of

394 the LTR (p=0.0219), while in the presence of AZD5582 combined with the *ING3*
395 knockout, the decrease in BRD4 levels was only significant over the R and U5 region of
396 the HIV-1 LTR (p=0.0159) (**Figure 7C, D**). Altogether, our CUT&Tag results
397 demonstrate that the pan-H4Ac and BRD4 levels are correlated at the HIV-1 LTR upon
398 *ING3* knockout with and without AZD5582 treatment.

399 In contrast to the pan-H4Ac and BRD4 CUT&Tag levels at the HIV-1 LTR that
400 change upon knockout of *ING3*, independent of LRA treatment, we find a striking
401 difference in markers for transcription initiation and elongation as mediated by the
402 phosphorylation of RNA Polymerase II C-terminal domain of Rpb1 (RNA-Pol2-S5p and
403 RNA-Pol2-S2p, respectively) [54] only in the condition when the *ING3* knockout is
404 combined with activation of the non-canonical NFκB pathway through AZD5582
405 treatment (**Figure 7E-H**). Specifically, we find that there is a striking, significant increase
406 in RNA-Pol2-S5p signal at the HIV-1 LTR (p=4.2827E-5), body of the provirus ("provirus
407 body") (p=8.943E-5), and the region downstream of the integrated HIV-1 provirus
408 ("downstream") (p=2.03E-5) only in the condition where cells that are knocked out for
409 *ING3* are additionally treated with AZD5582 (**Figure 7E, F**). In contrast, for the RNA-
410 Pol2-S2p signal in cells with a combination of *ING3* knockout and AZD5582 treatment,
411 we observed a significant increase in the RNA-Pol2-S2p signal in the provirus body
412 (p=0.0458) and downstream region (p=3.89E-5), but not over the LTR (**Figure 7G, H**).
413 Interestingly, in the intermediate condition of only *ING3* knockout, the signal of RNA-
414 Pol2-S2p is significantly reduced at the HIV-1 LTR (p=0.00583) (**Figure 7G, H**). This
415 reduction in RNA-Pol2-S2p signal might be partially explained by the concomitant

416 reduction we see in pan-H4Ac signal at the HIV-1 LTR in the *ING3* knockout condition
417 alone. The striking increase in HIV-1 reverse transcriptase activity in the combination
418 condition is concordant with our CUT&Tag results and suggest that the knockout of
419 *ING3* combines with stimulation of the non-canonical NFκB pathway by AZD5582 to
420 promote a potent increase in the RNA-Pol2-S5p and RNA-Pol2-S2p on the HIV-1
421 proviral genome.

422 As we observed the most significant RNA-Pol2-S5p level changes in the
423 combined *ING3* knockout and AZD5582 treatment condition, we next asked whether the
424 increasing RNA-Pol2-S5p levels was specific to the HIV-1 provirus or if this was
425 occurring genome-wide. We compared the RNA-Pol2-S5p signal in the combined *ING3*
426 knockout cells treated with AZD5582 to the control (NTC + DMSO) condition. We found
427 the RNA-Pol2-S5p peaks over the HIV-1 LTR, provirus body, and downstream region
428 were amongst the peaks with the most significant increase in RNA-Pol2-S5p signal
429 (**Figure 8A**). We then rank ordered all the RNA-Pol2-S5p peaks by Log_2-fold change
430 and found that out of the 2,547 total RNA-Pol2-S5p peaks, the top three peaks arranged
431 from highest to lowest fold change were the HIV-1 provirus body, the region
432 downstream of the HIV-1 integration site, and the HIV-1 LTR (**Figure 8B**). The two
433 RNA-Pol2-S5p peaks with a significant increase in signal and the next highest fold
434 change cover HCG27, a long non-coding RNA, and HIST2H4A – HIST2H4B, part of
435 histone cluster 2 in the human genome. The RNA-Pol2-S5p peak with the strongest
436 reduction in RNA-Pol2-S5p signal in *ING3* knockout cells treated with AZD5582 covers
437 PCGF3, a part of the Polycomb group PRC1-like complex (**Figure 8B**). Overall, this

438 suggests the increase in transcription of the HIV-1 provirus caused by *ING3* knockout in
439 combination with AZD5582 treatment, as correlated to the RNA-Pol2-S5p mark, is
440 highly specific and nearly unique in the human genome. Thus, the CUT&Tag data
441 reveal that *ING3* knockout results in a reduction in H4Ac and BRD4 levels over the HIV-
442 1 LTR and that *ING3* knockout acts in combination with AZD5582 treatment to
443 dramatically increase the transcriptional initiation and transcription elongation of the
444 HIV-1 provirus leading to latency reversal.
445

446 **Discussion**

447 The hypothesis underlying this work is that modulating multiple overlapping
448 mechanisms that control HIV-1 LTR-driven transcription will increase the potency and
449 specificity of HIV-1 latency reactivation. That is, the goal is to find pathways that target
450 potent transcriptional activation of latent HIV-1 proviruses with minimal global effects.
451 We designed and validated a modular CRISPR screening approach which uses the
452 incorporation of HIV-CRISPR genomes encoding sgRNAs into budding virions as a
453 direct readout of activation of the latent provirus. The Latency HIV-CRISPR screen uses
454 a sgRNA library of epigenetic regulatory genes and is paired with and without an LRA,
455 AZD5582, to identify HIV-1 latency factors that act independently and in combination
456 with AZD5582. We identified *ING3* as a gene whose knockout resulted in an enhanced
457 increase of viral reactivation only in the presence of AZD5582. Using automated
458 CUT&Tag, we observed that this enhancement is associated with active transcription
459 marks as demonstrated by increased levels of RNA-Pol2-Ser5p and RNA-Pol2-Ser2p at

460 the HIV-1 genome and mechanistically may be directly or indirectly dependent on a
461 reduction in histone H4 acetylation and BRD4 occupancy over the HIV-1 LTR. We also
462 identified CUL3 and multiple members of the NuA4 HAT complex as important for HIV-1
463 latency maintenance.

464 *Combinations of pathways with specificity for activating HIV-1 transcription*

465 We find that two independent mechanisms - *ING3* knockout and low-activating
466 dose of AZD5582 – which when combined, have unique, specific effects on the HIV-1
467 LTR and function together to efficiently activate HIV-1 transcription by increasing the
468 presence of initiated and elongating RNA-Pol2 at the LTR and within the body of the
469 HIV-1 provirus (**Figure 7**). Under these conditions used in our study, the RNA-Pol2-S5p
470 peaks with the highest fold change throughout the entire genome were at the HIV-1 LTR
471 and the provirus body (**Figure 8**). By CUT&Tag, RNA-Pol2-S5p appears as the primary
472 marker for HIV-1 transcription in the J-Lat 10.6 cell line and this may be a result of P-
473 TEFb, the major elongation factor for HIV-1 transcription, is a CTD kinase that can
474 phosphorylate Ser5 and Ser2 individually, but not simultaneously [55]. Our model
475 suggests that a reduction in NuA4 acetylation and BRD4-dependent occupancy at the
476 HIV-1 LTR is associated with enhanced transcription in response to *ING3* knockout and
477 activation of the non-canonical NFκB pathway.

478 We observed a reduction in histone acetylation and BRD4 recruitment to the HIV-
479 1 LTR that is concomitant with enhanced RNA-Pol2 initiation and elongation only upon
480 a combination of *ING3* knockout and AZD5582 treatment. This suggests the HIV-1
481 provirus may be subject to unexpected transcriptional control. In most mammalian

482 transcriptional units driven by RNA-Pol2, NuA4 HAT is predominantly localized to
483 promoters of active genes, specifically around the transcription start sites [56-58]. The
484 NuA4 HAT preferentially acetylates histone H4 [59] and this activity often impacts the
485 regulation of gene expression by activating transcription. Additionally, BRD4 binds to
486 acetylated chromatin [60], remains chromatin bound during mitosis [61, 62], and
487 positively regulates mammalian transcription elongation through interaction with P-TEFb
488 [36, 63]. Moreover, recruitment of other HAT complexes such as p300/CBP and P/CAF
489 to the HIV-1 LTR followed by subsequent acetylation is associated with stimulation,
490 rather than silencing, of HIV-1 transcription [64-70]. Additionally, using *in vitro*
491 nucleosome-assembled templates in a Tat-independent system, the NuA4 HAT
492 activates HIV-1 transcription [71]. Conversely, in the presence of Tat, the NuA4 HAT
493 complex has been implicated in silencing of HIV-1 transcription. For example, in both a
494 primary CD4+ T cell model and cells from ART-treated people living with HIV-1, the
495 absence of KAT5, the catalytic component of the NuA4 HAT complex, promotes
496 activation of HIV-1 transcription as a result of reduced H4 acetylation and BRD4 long
497 isoform occupancy, and increased levels of the Super Elongation Complex (SEC)
498 members at the HIV-1 LTR [9]. Furthermore, BRD4 has been demonstrated to not be
499 required for HIV-1 transcription in the presence of Tat in HeLa cells [36] and has the
500 potential to compete with Tat for binding to P-TEFb [16, 36]. Perhaps a competition
501 model could explain why the reduced levels of acetylation and BRD4 we observed upon
502 *ING3* knockout and AZD5582 treatment are associated with increases in HIV-1
503 transcription. Importantly, loss of BRD4 is not correlated with any changed in the

504 binding of CDK9, a subunit of P-TEFb [72], thus the reduced levels of BRD4 are unlikely
505 to be directly impacting P-TEFb binding. Instead, we propose a model in which the
506 knockout of *ING3* leads to a decrease of H4 acetylation and BRD4, which enhances Tat
507 recruitment of P-TEFb to TAR due to an increase in spatial opportunity for chromatin
508 binding. In addition, the treatment of a low-activating dose of AZD5582 leads to
509 recruitment of poised and active RNA-Pol2 at the HIV-1 LTR. Thus, upon the unique
510 combination of *ING3* knockout and AZD5582 treatment, we observe the potent and
511 nearly specific increase in viral transcription. Interestingly, our findings are consistent
512 with this observation as our Latency HIV-CRISPR screen identified multiple members of
513 the NuA4 HAT complex, including KAT5, as top candidates and all the candidates were
514 validated as latency maintenance factors through individual knockouts. In fact, our
515 screen suggests that not only the catalytic subunit, but the NuA4 HAT complex
516 altogether regulates HIV-1 transcription negatively.

517 We observed a reduction in H4 acetylation across the entire HIV-1 LTR in
518 response to *ING3* knockout, but in the presence of AZD5582 we see the most
519 significant reduction of H4Ac signal and BRD4 occupancy at the R and U5 region which
520 includes the HIV-1 transcription start site. This observation suggests, the increase in
521 accessibility of the HIV-1 transcription start site when *ING3* knockout combined with
522 AZD5582 treatment likely promotes both transcription initiation and elongation,
523 culminating in the enhanced viral reactivation we observe in both J-Lat cells and primary
524 CD4+ T cell HIV-1 latency models. Additionally, the dosage of AZD5582 used was a
525 low-reactivating dose, suggesting that by inhibiting the NuA4 complex in parallel, it may

526 be possible to efficiently activate HIV-1 transcription while causing minimal disruptions
527 to a host system. HIV-1 is subject to complex transcriptional regulation, and these
528 results highlight the importance of simultaneously examining multiple mechanisms to
529 identify opportunities to specifically stimulate transcription of latent HIV-1 proviruses.
530 These results are similar in concept to a recent study that found that the combination of
531 AZD5582 and I-BET151 uniquely activated HIV-1 transcription in a Jurkat model of
532 latency [73].

533 In support of the hypothesis that these mechanisms are nearly unique to the HIV-
534 1 LTR, relatively few loci in the host genome showed a significant increase in RNA-
535 Pol2-S5p occupancy when *ING3* knockout is combined with a low-activating dose
536 treatment of AZD5582. One of these regions is downstream of the HIV-1 provirus
537 integration site in J-Lat 10.6 cells and part of the *SEC16A* gene (**Figure 8**). Activation of
538 human genes near or at the integrated provirus due to active transcription from an
539 integrated provirus is a likely scenario as HIV-1 preferentially integrates into highly
540 transcribed genes [74], and would be an unavoidable consequence of any reactivation
541 strategy used for eradicating the latent HIV-1 reservoir. In the combined condition of
542 *ING3* knockout and AZD5582 treatment, two other loci, a region of histone cluster 2
543 spanning HIST2H4A – HIST2H4B and a region overlapping with the long-noncoding
544 RNA, HCG27, also showed statistically significant, large fold changes in RNA-Pol2-S5p
545 levels, but these changes were not as prominent as those observed over the HIV-1
546 provirus (**Figure 8**). In addition, we observed the gene PCGF3 had significantly reduced
547 RNA-Pol2-S5p occupancy which could potentially to contribute to latency reversal as it

548 is part of the non-canonical Polycomb group RING finger 3/5-PRC1 complex with
549 silencing function [75] and is involved in the recruitment of PRC1 and PRC2 which have
550 been shown to contribute to HIV-1 proviral silencing [8, 10, 76].

551 *Comparison to other HIV latency screens*

552 Our Latency HIV-CRISPR screening strategy is a unique approach to identify
553 factors involved in HIV-1 latency. However, previous screens have also explored HIV-1
554 latency factors using gene knockout, knockdown, or silencing screening [10, 20-27].
555 Generally, these previous screens used whole genome sgRNA libraries which make
556 them unbiased for specific pathways, but this also limits the strength in statistical power
557 to determine gene hits. Nonetheless, these previous screens have uncovered an
558 exciting breadth of HIV-1 latency factors from the mTOR pathway [20] to proteasome
559 related genes [23, 25] to the non-canonical NFκB pathway [27]. As epigenetics plays an
560 important role in HIV-1 latency and it is still under investigation, we focused our Latency
561 HIV-CRISPR screen for epigenetic regulatory factors by using a small, custom designed
562 sgRNA library. Additionally, a smaller library can increase the dynamic range of a
563 screen [77]. Our screen also relies on the HIV-CRISPR vector [30] to perform a high-
564 throughput screen, which uses HIV-1 replication, rather than another reporter, as the
565 direct readout of the screen. The difference in readout from other screens including
566 screens with epigenetic hits [10, 22, 26] can result in different gene hits being
567 highlighted. Another challenge of studying mechanisms of HIV-1 latency is the
568 interaction of complex mechanisms in parallel and to address this using a CRISPR
569 screen approach, we combined the screen with a low-activating dose of LRA treatment.

570 By focusing our sgRNA library on epigenetic regulators and performing our screen with
571 and without AZD5582 treatment, we identified a unique combination of modifications
572 that synergize to stimulate HIV-1 transcriptional initiation and elongation.

573 A paper published while this manuscript was being prepared used a similar
574 strategy of CRISPR screening in the presence of low-activating doses of LRA, but with
575 a whole-genome guideRNA library [78]. Dai et al found that *BRD2* knockout synergized
576 with AZD5582 [78], which likely falls within the same pathway identified in our study. In
577 fact, in our screen results, *BRD2* also was a highly ranked gene hit in the presence of
578 AZD6682 (rank #19 in the J-Lat 5A8 cell screen and #55 in the J-Lat 10.6 cell screen)
579 (**Supplementary Table 5**). Thus, by exploring the combination of low-activating doses
580 of LRAs with CRISPR based screens, the field can identify pathways leading to
581 improvements in the specificity and potency of novel LRAs towards a curative treatment
582 strategy that eradicates the HIV-1 latent pool.

583

584 **Acknowledgements**

585 We thank Terry Hafer and Carley Gray for critical feedback of this manuscript, Jessie
586 Kulsuptrakul for technical assistance, and members of the Emerman lab for helpful
587 suggestions. We thank Steve Hahn and B. Matija Peterlin for helpful discussions. We
588 thank Warner Greene at Gladstone Institute of Virology and Immunology and University
589 of California, San Francisco, San Francisco, CA, USA for sharing the J-Lat 5A8 cells
590 and Darell Bigner at Duke University, Durham, NC, USA for sharing the H80 cells. We
591 thank Lucas Carter for assistance in assembly of the HuEpi library, Jackson Peterson

592 for discussions on the primary cell HIV-1 latency model, Daryl Humes and Hannah Itell
593 for discussions on primary cell protocols, and Jorja Henikoff, Matt Fitzgibbon and Pritha
594 Chanana at the FHCC for bioinformatics support. This work was supported by DP1
595 DA051110 (ME), CARE 1UM1-A1-164567 (ME, EPB), University of Washington (UW)
596 Viral Pathogenesis training grant NIH T32 AI 083203 (EH), National Science Foundation
597 Graduate Research Fellowship DGE-1256082 and DGE-1762114 (EH), Hartwell
598 Foundation Postdoctoral Fellowship (DHJ), R01 DK119270-01 (PJP), NIDDK-
599 U54DK106829 (PJP), NIAID R01 AI143381 (EPB), NIDA R61 DA047023 (EPB),
600 Howard Hughes Medical Institute (SH), and R01 AI147877 (MO). Construction of the
601 HuEpi library was supported by a Fred Hutchinson Cancer Center Pathogen Associated
602 Malignancy Integrated Research Center award. This research was supported by the
603 Genomics, Bioinformatics, and Flow Cytometry Shared Resource, RRID:SCR_022606,
604 of the Fred Hutch/University of Washington Cancer Consortium (P30 CA015704).
605

606 **Figure Legends**
607
608 **Figure 1. The Latency HIV-CRISPR screen.**
609 **(A)** Schematic summarizing the Latency HIV-CRISPR screen in J-Lat cell lines showing
610 the latent, integrated provirus and the HIV-CRISPR vector which delivers Cas9 and a
611 sgRNA and produces a packageable genomic RNA. Red boxes represent the gene or
612 sgRNA targeting the gene of interest; gray boxes represent functional HIV-1 LTRs at
613 both sides of the vector and provirus; triangles represent internal promoters for sgRNA
614 and Cas9 transcription. **(B)** Categorical distribution of the genes targeted by the Human
615 Epigenome (HuEpi) sgRNA library. **(C)** Metascape Gene Ontology (GO) analysis [43] of
616 the genes targeted by the HuEpi sgRNA library. **(D)** Summary of workflow from the
617 generation of the pool of J-Lat HuEpi knockout cells to the sequencing and comparison
618 of the abundance of guideRNAs found in the viral RNA (vRNA) pool versus the genomic
619 DNA (gDNA) pool. GuideRNAs enriched in the viral supernatant RNA relative to the
620 genomic DNA represent the gene(s) that upon knockout result in latency reversal.
621
622 **Figure 2. GuideRNA level enrichment for known and novel genes of interest in the**
623 **Latency HIV-CRISPR screen.**
624 **(A)** GuideRNA enrichment (log_2 of fold change) in both J-Lat cell lines for the genes
625 targeted by the HuEpi sgRNA library compared to the Non-Targeting Control (NTC)
626 guides. For statistical analysis, the HuEpi gene sgRNAs are compared to the NTC
627 control. Welch's t-test, p-value < 0.0001. **(B)** GuideRNA level enrichment of known HIV-
628 1 latency maintenance factors BRD4, KAT5, and PRC2 complex members (EZH2,
629 SUZ12, and EED) in the Latency HIV-CRISPR screen. For statistical analysis, all
630 conditions are compared to the NTC control. Welch's t-test, p-value =<0.05 = *, =<0.05
631 = **, =<0.001 = ***.
632
633 **Figure 3. The Latency HIV-CRISPR screen in J-Lat 10.6 and J-Lat 5A8 cells**
634 **identifies a set of mutual, novel hits.**
635 **(A)** The $-log_{10}$ of the MAGeCK scores for each gene targeted by the HuEpi sgRNA
636 library (black circles and red triangles) and NTCs (gray squares) are calculated and
637 displayed. Gene names are labelled for hits that have a <10% false discovery rate
638 (FDR) in both J-Lat cell lines (center of Venn diagram in (B)); red triangles represent
639 members of the NuA4 HAT complex and SRCAP complex. NTCs are artificial NTC
640 genes designed by iterative binning of NTC sgRNA sequences (see Methods). Genes
641 are randomized on the x-axis, but the same order is used for both right and left panels.
642 The y-axis is the inverse log_{10} of the MAGeCK score. **(B)** Top hit genes (cut off of <10%
643 FDR) in common and unique to each J-Lat cell line are ordered by significance and
644 FDR with the top of the list having the highest significance and lowest FDR. **(C)**
645 Metascape GO analysis [43] of the gene hits with a <10% FDR in each J-Lat cell line.
646 (**D)** Analysis of the $-log_{10}$ of the MAGeCK scores of the genes overlapping and unique to
647 the NuA4 HAT and SRCAP complex compared to the NTCs. The higher the number,
648 the more statistically significant it is of a hit. Red font is for genes that score higher than
649 the average NTC score.

650
651 **Figure 4. Validation of top hits from Latency HIV-CRISPR screen.**
652 **(A)** Validation of the top 9 gene hits of the Latency HIV-CRISPR screen was performed
653 by individually knocking out each J-Lat cell line with two different guide RNAs and
654 measuring viral reactivation by quantifying HIV-1 reverse transcriptase activity of the
655 viral supernatant. *NFκBIA* knockout is a positive control. The reverse transcriptase
656 activity from released virions was normalized to basal activity from the NTC knockout.
657 For each for the knockout cell lines, ICE analysis was performed and the average
658 knockout is shown in pie charts. Multiple unpaired t-tests, p-value =<0.05 = *. **(B)** *CUL3*
659 knockout resulted in significant viral reactivation in a primary CD4+ T cell model of HIV-
660 1 latency using cells from four healthy donors. Viral reactivation was measured by flow
661 cytometry and normalized to the *AAVS1* knockout cells. Paired t-test, p-value =<0.05 =
662 *, =<0.05 = **.
663
664 **Figure 5. LRA Latency HIV-CRISPR screen identifies ING3 in combination with**
665 **AZD5582 as a HIV-1 latency maintenance factor.**
666 **(A)** *ING3* is the top hit of the LRA Latency HIV-CRISPR screen. The Latency HIV-
667 CRISPR screen HuEpi knockout cells were treated with a low activating dose (10 nM) of
668 AZD5582. The -$\log_{10}$ of the MAGeCK score (on the y-axis) for each gene targeted by
669 the HuEpi sgRNA library (black circles) and NTCs (gray squares) are calculated and
670 displayed. NTCs are artificial NTC genes designed by iterative binning of NTC sgRNA
671 sequences (see Methods). Genes are randomized on the x-axis, but the same order is
672 used for both right and left panels. **(B)** Comparison of the Latency HIV-CRISPR screen
673 by MAGeCK score in the presence (y-axis) and absence of AZD5582 (x-axis) with
674 HuEpi genes (circles) and NTCs (gray squares). The data for the screen without an LRA
675 (x-axis) is from Figure 3 as these two screens were performed in parallel. The genes
676 unique to each screen are closest to the respective axis and the genes that are in
677 common to both screens are at the center. *ING3* is highlighted in periwinkle and *CUL3*
678 in green.
679
680 **Figure 6. Validation of ING3 in combination with AZD5582 as a HIV-1 latency**
681 **maintenance factor.**
682 **(A)** HIV-1 reverse transcriptase activity (y-axis) of the viral supernatant of NTC sgRNA
683 transduction or *ING3* knockout in J-Lat 10.6 and 5A8 treated with 10 nM AZD5582 or an
684 equivalent volume of DMSO. *ING3* knockout and AZD5582 treatment combine to result
685 in a significant increase in viral reactivation. Paired t-test, p-value =<0.05 = *, =<0.05 =
686 **. **(B)** Representative flow cytometry plots of primary CD4+ T cell HIV-1 latency model
687 cells that are *AAVS1* or *ING3* knockouts treated with DMSO or 1 μM AZD5582
688 treatment. Thy1.2-, GFP- cells (quadrant 4) are uninfected; Thy1.2+, GFP- (quadrant 3)
689 cells are infected with the dual reporter HIV-1 virus and latent; Thy1.2+, GFP+ cells
690 (quadrant 2) are infected and reactivated. **(C)** Four independent knockouts of *AAVS1*
691 and *ING3* in primary CD4+ T cell HIV-1 latency model cells were performed in two
692 healthy donors (three knockouts in one donor, one knockout in another donor) and each
693 pool of knockout cells were treated with DMSO or 1 μM AZD5582. Knockout of *ING3*

694 and AZD5582 treatment combined resulted in significant reactivation compared to
695 knockout of *AAVS1*. Paired t-test, p-value =<0.05 = *. **(D)** Western blot showing similar
696 p52 levels are detected in the control and ING3 knockout J-Lat 10.6 and 5A8 cell lines
697 upon treatment of 10 nM AZD5582. Activation of the non-canonical NFκB (NFκB2)
698 pathway is marked by a decrease in p100 and an increase in the cleaved product of
699 p52.
700
701 **Figure 7. *ING3* knockout decreases pan-H4Ac and BRD4 levels and stimulates**
702 **HIV-1 transcriptional initiation and elongation upon addition of AZD5582.**
703 **(A)** Genome browser tracks centered over the HIV-1 LTR showing the pan-H4Ac signal
704 decreases in the *ING3* knockout alone and in combination with AZD5582 conditions.
705 The y-axis represents read count. Because the HIV-1 LTR sequence is identical
706 between 5' LTR vs. the 3' LTR, the CUT&Tag reads are combined onto one LTR. The
707 LTR is subdivided into three regions: U3, R (containing the transcription start site), and
708 U5. As quality control, we determined the signal levels of pan-H4Ac from the CUT&Tag
709 data and confirmed the replicates of the antibody was most highly correlated amongst
710 the pan-H4Ac replicates (**Supplemental Figure 3A**). **(B)** Box plot showing the pan-
711 H4Ac levels quantified over the full LTR including the U3 region and the R+U5 regions
712 that include the transcriptional start site. The y-axis is the pan-H4Ac base pair coverage
713 normalized to the total base pair coverage across the genome. Blue represents the
714 transduction of NTC sgRNA with treatment of DMSO; yellow represents the
715 transduction of NTC sgRNA with a treatment of 10 nM AZD5582; orange represents
716 *ING3* knockout with treatment of DMSO; red represents *ING3* knockout with treatment
717 of 10 nM AZD5582. Replicates for IgG n=18 and pan-H4Ac n=24. For statistical
718 analysis, all conditions are compared to the NTC knockout and DMSO treatment
719 control. P-value <0.05 = *, <0.005=**. **(C)** Genome browser tracks showing BRD4 levels
720 decrease in the *ING3* knockout alone and in combination with AZD5582 conditions. As
721 quality control, we determined the signal levels of BRD4 from the CUT&Tag data and
722 confirmed the replicates of the antibody was most highly correlated amongst the BRD4
723 replicates (**Supplemental Figure 3A**). **(D)** Same as (B) but quantifying BRD4 levels.
724 Replicates for BRD4 n=16. **(E)** Genome browser tracks showing RNA-Pol2-S5p levels
725 increase at the HIV-1 LTR, as well as the body of the provirus downstream of the 5' LTR
726 ("provirus body"), and the region of the host genome downstream of the 3' LTR of the
727 integrated provirus ("downstream") upon *ING3* knockout and AZD5582 treatment
728 combined. As quality control, we determined the signal levels of RNA-Pol2-S5p from the
729 CUT&Tag data and confirmed the replicates of the antibody was most highly correlated
730 amongst the RNA-Pol2-S5p replicates (**Supplemental Figure 3B**). **(F)** Box plot showing
731 the quantification of the RNA-Pol2-S5p CUT&Tag signal over the HIV-1 LTR, as well as
732 the body of the provirus, and the region of the host genome downstream of the provirus.
733 The y-axis is the RNA-Pol2-S5p base pair coverage normalized to the total base pair
734 coverage across the genome. Blue represents the transduction of NTC sgRNA with
735 treatment of DMSO; yellow represents the transduction of NTC sgRNA with a treatment
736 of 10 nM AZD5582; orange represents *ING3* knockout with treatment of DMSO; red
737 represents *ING3* knockout with treatment of 10 nM AZD5582. Replicates for RNA-Pol2-

S5p n=13. For statistical analysis, all conditions are compared to the NTC knockout and DMSO treatment control. P-value <0.05 = *, <0.005=**, <0.0005=***. **(G)** Genome browser tracks showing RNA-Pol2-S2p levels increase over the body of the HIV-1 provirus as well as the host genome downstream of the provirus upon *ING3* knockout and AZD5582 treatment combined. As quality control, we determined the signal levels of RNA-Pol2-S2p from the CUT&Tag data and confirmed the replicates of the antibody was most highly correlated amongst the RNA-Pol2-S2p replicates (**Supplemental Figure 3B**). **(H)** Same as (F) but quantifying RNA-Pol2-S2p levels. Replicates for RNA-Pol2-S2p n=17.

Figure 8. Changes in RNA-Pol2-S5p levels upon *ING3* knockout combined with AZD5582 treatment are nearly unique to the HIV-1 provirus.
(A) Volcano plot comparing RNA-Pol2-S5p peaks between the NTC KO + DMSO (negative control) and ING3 KO + AZD5582 conditions. Highlighted peaks over the HIV-1 LTR (magenta circle), the body of the provirus (purple circle), and downstream region of HIV-1 provirus (teal circle) are the regions of the highest RNA-Pol2-S5p fold change and are highly significant. Other regions with an absolute $\log_2$ fold change greater than 1 and a $-\log_{10}$ adjusted p-value > 2 are highlighted in red. **(B)** Scatter plot showing all of the RNA-Pol2-S5p peaks rank ordered by fold change. Peaks are colored as in (A). The top three regions are the HIV-1 LTR, body of the HIV-1 provirus, and downstream region of the HIV-1 provirus. The next two regions overlap *HCG27* and the histone cluster 2 spanning HIST2H4A-HIST2H4B. The region with the greatest reduction in RNA-Pol2-S5p signal overlaps *PCGF3*.

762 **Materials and Methods**
763
764 **J-Lat wildtype, clonal knockout, and pooled knockout cells**
765 The HIV-1 latency cell line J-Lat 5A8 [29] and J-Lat 10.6 [28] were grown in RPMI-1640
766 medium (Thermo Fisher Scientific) supplemented with 10% Fetal Bovine Serum (FBS),
767 Penicillin-Streptomycin (Pen/Strep), and 10 mM HEPES. In order to use these cells for
768 screening with HIV-CRISPR, we performed CRISPR/Cas9-mediated knockout of Zinc
769 Antiviral Protein (ZAP) [30] by electroporation of the J-Lat 10.6 and 5A8 cells with a
770 Gene Knockout v2 kit (GKOv2) for ZAP (Synthego, Redwood City, CA) complexed with
771 1 μL of 20 μM Cas9-NLS (UC Berkeley Macro Lab). 5 days post electroporation, the
772 cells were single cell sorted into a 96-well U-bottom plate (Sony MA900 Multi-
773 Application Cell Sorter – Fred Hutch Flow Cytometry shared resource) and individual
774 clones with biallelic knockouts of ZAP were used for subsequent Latency HIV-CRISPR
775 screens. J-Lat cells with HIV-CRISPR KO pools targeting NFKBIA, KAT5, CUL3,
776 ACTL6A, VPS72, DNMT1, DMAP1, SRCAP, YEATS4, and two non-targeting controls
777 (**Supplemental Table 6**) were generated by transduction of lentivirus and subsequent
778 0.4 μg/mL puromycin selection for 10-14 days. To generate the CRISPR/Cas9-edited
779 knockout pools, the sgRNAs that were the most overrepresented in the viral
780 supernatant (highest combined p-value) of the Latency HIV-CRISPR screen were
781 selected. Cell lines were determined to be mycoplasma free by the Fred Hutch
782 Specimen Processing/Research Cell Bank shared resource.
783
784 **Plasmids**
785 HIV-CRISPR plasmid was previously described [30]. HIV-CRISPR constructs targeting
786 genes of interest were cloned by annealing complementary oligos (**Supplemental**
787 **Table 6**) with overhangs that allow directional cloning into HIV-CRISPR using the
788 BsmBI restriction sites. pMD2.G and psPAX2 plasmids were gifts from Didier Trono
789 (Addgene #12259 and #12260, respectively). pMD2.Cocal plasmid was a gift from
790 Hans-Peter Kiem [79]. lentiCRISPRv2 plasmid was a gift from Feng Zhang (Addgene
791 #52961). The pNL4-3-Δ6-dreGFP-CD90 was previously described [50].
792
793 **Human Epigenome CRISPR/Cas9 sgRNA Library Construction**
794 The Human Epigenome (HuEpi) sgRNA library is composed of 841 genes of which 778
795 genes derive from the database Epifactor [32] and 63 genes were hand selected. For
796 most genes, six sgRNA sequences were generated using GUIDES (Graphical User
797 Interface for DNA Editing Screens) [80]. Two genes (HEATR1 and MCM2) have
798 fourteen guides and one gene (UBE2N) has one guide. 252 non-targeting sgRNAs
799 sourced from GeCKO v2.0 library [33] were also included resulting in a generated
800 library of a total of 5,309 guides. The HuEpi sgRNA was synthesized (Twist
801 Biosciences, San Francisco, CA) and cloned into HIV-CRISPR. Oligo pools were
802 amplified using Phusion High-Fidelity DNA Polymerase (NEB) combined with 1 ng of
803 pooled oligo template, primers ArrayF and ArrayR (ArrayF primer:
804 TAACTTGAAAGTATTTCGATTTCTTGGCTTTATATATCTTGTGGAAAGGACGAAACA
805 CCG and ArrayR primer:

806 ACTTTTTCAAGTTGATAACGGACTAGCCTTATTTTAACTTGCTATTTCT
807 AGCTCTAAAAC), an annealing temperature of 59°C, an extension time of 20 s, and 25
808 cycles. Following PCR amplification, a 140 bp amplicon was gel-purified and cloned into
809 BsmBI (NEB; R0580) digested HIVCRISPR using Gibson Assembly (NEB; E2611S).
810 Each Gibson reaction was carried out at 50°C for 60 min. Drop dialysis was performed
811 on each Gibson reaction according to the manufacturer's protocol using a Type-VS
812 Millipore membrane (VSWP 02500). 5 µl of the reaction was used to transform 25 µl of
813 Endura electrocompetent cells (Lucigen; 60242-2) according to the manufacturer's
814 protocol using a Gene Pulser (BioRad). To ensure adequate representation, sufficient
815 parallel transformations were performed and plated onto carbenicillin containing LB
816 agarose 245 mm x 245 mm plates (Thermo Fisher) at 300-times the total number of
817 oligos of each library pool. After overnight growth at 37°C, colonies were scraped off,
818 pelleted, and used for plasmid DNA preps using the Endotoxin-Free Nucleobond
819 Plasmid Midiprep kit (Takara Bio; 740422.10). The HuEpi library was sequenced and
820 contains all 5,309 sgRNAs included in the synthesis (GSE215430).
821
822 **Lentivirus Production**
823 293T cells (ATCC;CRL-3216) cultured in DMEM (Thermo Fisher Scientific)
824 supplemented with 10% FBS and PenStrep were plated at 2E5 cells/mL in 2 mL in 6-
825 well plates one day prior to transfection. Transfection is performed using TransIT-LT1
826 reagent (Mirus Bio LLC; MIR2300) with 3 uL of transfection reagent per µg of DNA. For
827 lentiviral preps, 293Ts were transfected with 667 ng lentiviral plasmid, 500 ng psPAX2,
828 and 333 ng pMD2.G. One day post-transfection, media was replaced. Two- or three-
829 days post-transfection, viral supernatants were filtered through a 0.2 µm filter (Thermo
830 Scientific; 720-1320). For HuEpi library lentiviral preps, the same transfection of 293Ts
831 was performed and supernatants from forty 6-well plates were combined and
832 concentrated by ultracentrifugation. About 30 mL of supernatant are aliquoted into a
833 polypropylene tube (Beckman Coulter; 326823) and underlaid with sterile-filtered 20%
834 sucrose (20% sucrose, 1 mM EDTA, 20 mM HEPES, 100 mM NaCl, distilled water).
835 Each of the polypropylene tubes are placed in a swinging bucket and spun in a SW 28
836 rotor at 23,000 rpm for 1 hour at 4°C in a Beckman Coulter Optima L-90K
837 Ultracentrifuge. Supernatants were decanted and pellets are resuspended in DMEM or
838 RPMI over several hours at 4°C. Concentrated lentivirus was used immediately or
839 aliquots were made and stored at -80°C. All lentiviral transductions were performed in
840 the presence of 20 µg/mL DEAE-Dextran (Sigma-Alrdich; D9885). For generating pNL4-
841 3-Δ6-dreGFP-CD90 stocks, the procedure was the same as the lentiviral preps except
842 that 293Ts were transfected with 900 ng lentiviral plasmid, 450 ng psPAX2, and 150 ng
843 pMD2.Cocal.
844
845 **LRA and no LRA Latency HIV-CRISPR Screening**
846 The HuEpi library lentiviral preps were titered by a colony-forming assay in TZM-bl cells
847 (NIH AIDS Reagent Program; ARP-8129) and used to transduce J-Lat 10.6 and J-Lat
848 5A8 cells at an MOI of 0.4. For the transduction, 3E6 cells per replicate (>500x
849 coverage of the HuEpi library) was used and the spinoculation was performed at

850 1100xg for 30 min in the presence of 20 μg/mL DEAE-Dextran. Cells were selected in
851 puromycin (0.4 μg/mL) for 10-14 days. In preparation for the LRA screen, AZD5582
852 dihydrochloride (Tocris; 5141) was resuspended in DMSO to 1 mM stocks. Subsequent
853 dilutions are performed in RPMI and used immediately. Upon completion of selection,
854 for the LRA screen, 3E6 cells per replicate per cell line were treated with 10 nM
855 AZD5582 for 24 hours. Cells and supernatants were collected post selection or post
856 treatment. Cells were washed once with DPBS (Gibco; 14190144) and cell pellets were
857 stored at -20°C. Genomic DNA was extracted from cell pellets with the QIAamp DNA
858 Blood Midi Kit (Qiagen; 51183) and genomic DNA was eluted in distilled water. Viral
859 supernatants were spun at 1100xg to remove cell debris, filtered through a 0.22 μm filter
860 (Millipore Sigma, SE1M179M6), overlaid on a 20% sucrose cushion, and concentrated
861 in a SW 28 rotor for 1 hour at 4°C. The pellet is resuspended in RPMI and stored at -
862 80°C. Viral RNA was extracted from the concentrated virus with the QIAamp Viral RNA
863 Mini Kit (Qiagen, 52904). The sgRNA sequences found in the genomic DNA and viral
864 RNA samples were amplified by PCR (Agilent; 600677) and RT-PCR (Invitrogen;
865 18064014), respectively, using HIV-CRISPR specific primers. A second round of PCR is
866 performed to barcode and prepare the libraries for Illumina sequencing (**Supplemental**
867 **Table 6**). Each amplicon was cleaned up using double-sided bead clean-up (Beckman
868 Coulter; A63880), quantified with a Qubit dsDNA HS Assay Kit (Invitrogen; Q32854),
869 and pooled to 10 nM for each library. Library pools are sequenced on a single lane of an
870 Illumina HiSeq 2500 in Rapid Run mode (Fred Hutch Genomics and Bioinformatics
871 shared resource).
872
873 **Screen Analysis**
874 Raw sequencing data is available as a GEO DataSet (GSE215430). Library pools are
875 demultiplexed, reads are assigned to respective samples, trimmed, and aligned to the
876 HuEpi library via Bowtie [81]. An artificial NTC sgRNA gene set the same size as the
877 HuEpi library was generated by iteratively binning the NTC sgRNA sequences. Analysis
878 of the screen to determine relative enrichment or depletion of the sgRNAs and genes
879 were performed using the MAGeCK statistical package [35].
880
881 **Western Blotting/Immunoblotting**
882 Cells were harvested and washed once with ice cold phosphate-buffered saline (PBS)
883 and pelleted by centrifugation (300 x g for 3 min). Whole cell lysate was extracted on ice
884 by first resuspending the cell pellet with Pierce IP Lysis Buffer (ThermoFisher Scientific;
885 87787) supplemented with cOmplete protease inhibitor cocktail (Roche; 11697498001).
886 The samples were then incubated on ice for 10 min with brief vortexing every 2-3 min
887 and followed by a centrifugation at 16,000 x g for 20 min at 4°C. To prepare the
888 samples, add 4x NuPAGE LDS Sample Buffer (ThermoFisher Scientific; NP0008)
889 containing 5% 2-Mercaptoethanol (Millipore Sigma; M3148) and boil the samples at
890 95°C for 5 min. Lysates were resolved on a NuPAGE 4-12% Bis-Tris pre-cast gel
891 (ThermoFisher Scientific; NP0336) and transferred to nitrocellulose membranes (Biorad;
892 1620115). Blocking was performed for 1 hr at room temperature using 5% milk/0.1%
893 Tween-20 added to Tris-buffered saline (TBS) (20 mM Tris base and 150 mM NaCl at

894 pH 7.6). Immunoblotting was performed using the primary antibodies CUL3 (Cell
895 Signaling; 2759) at 1:1000, NFkB2 (Cell Signaling; 4882) at 1:1000, and viniculin (Santa
896 Cruz; sc-25336) at 1:5000. Membranes were washed with TBST 6 times for 5 min each.
897 The following secondary antibodies were used at a 1:5000 dilution: goat anti-rabbit IgG-
898 HRP (R&D Systems; HAF008) and goat anti-mouse IgG-HRP (R&D Systems; HAF007).
899 Membranes were developed with SuperSignal West Femto Maximum Sensitivity
900 Substrate (Thermo Fisher; 34095) and visualized on a BioRad Chemidoc MP Imaging
901 System.
902
903 **Genomic Editing Analysis**
904 Knockout cells were harvested and DNA was extracted using the QIAamp DNA Blood
905 Mini Kit (Qiagen; 51104). Primers from each targeted locus (**Supplemental Table 6**)
906 were used to amplify the edited loci and the PCR was performed with either Platinum
907 Taq DNA Polymerase High Fidelity (ThermoFisher Scientific; 11304011) or Q5 High-
908 Fidelity DNA Polymerase (NEB; M0491S). Sanger sequencing was performed on PCR
909 amplicons (Fred Hutch Genomics shared resource) using a sequencing primer
910 (**Supplemental Table 6**) and results were analyzed by Inference of CRISPR Edits (ICE)
911 [44] to determine gene editing outcome.
912
913 **Virus Release (RT assay)**
914 Clarified viral supernatants are harvested and reverse transcriptase activity was
915 measured using the HIV-1 reverse transcriptase (RT) activity assay as previously
916 described [82, 83]. A standard curve is generated for all assays using a titered stock of
917 HIV-1_{LAI} that was aliquoted at and stored at -80°C.
918
919 **Ethics Statement**
920 All primary cell data is from anonymous blood donors and is classified as "human
921 subjects exempt" research by the Fred Hutchinson Cancer Center Institutional Review
922 Boards, according to National Institutes of Health (NIH) guidelines
923 (http://grants.nih.gov/grants/policy/hs/faqs_aps_definitions.htm). No animal work was
924 done.
925
926 **Primary CD4+ T Cell Latency Model and Knockout**
927 Used leukocyte filters from healthy donors were obtained from Bloodworks Northwest
928 and total peripheral blood mononuclear cells (PBMCs) were isolated by purification over
929 Ficoll (Millipore Sigma; GE17-1440-02). CD4+ T cells were isolated using magnetic
930 negative selection (StemCell Technologies; 17952) and used immediately or frozen for
931 storage in liquid nitrogen. CD4+ T cells were activated using anti-CD2, CD3, and CD28
932 beads (Miltenyi Biotec; 130-091-441) for 2 days and grown in RPMI-1640 medium
933 (Thermo Fisher Scientific) supplemented with 10% Fetal Bovine Serum (FBS),
934 Penicillin-Streptomycin (Pen/Strep), 1x GlutaMAX (ThermoFisher Scientific; 35050061),
935 10 mM HEPES, 100 U/mL human interleukin-2 (Millipore Sigma; 11011456001), 2
936 ng/mL human interleukin-7 (Peptrotech; 200-07), and 2 ng/mL human interleukin-15
937 (Peprotech; 200-15). The beads were then removed by magnetic separation and cells

938 were spinoculated with HIV-GFP-Thy1.2 (pNL4-3-Δ6-dreGFP-CD90) and 8 ug/mL
939 polybrene (Millipore Sigma; TR-1003-G) for 2 hrs at 1100 x g. Spinoculated cells were
940 then resuspended in fresh media with IL-2, IL-7, and IL-15 and incubated for 3 days
941 before actively infected cells (Thy1.2+) were isolated by magnetic positive selection
942 (Stem Cell Technologies; 18951). Infected cells (Thy1.2+) are maintained for 2 days
943 before knockout of AAVS1, CUL3, and ING3 using GKOv2 kits from Synthego. crRNPs
944 for each gene of interest were generated as described previously in the Knockout Cell
945 Clones and Pools section except that supplemented P3 buffer (Lonza; V4SP-3096) is
946 used instead of SE buffer. For each electroporation, 1.5E6 cells were pelleted by
947 centrifugation at 100 x g for 10 min at 25°C, washed once with PBS, pelleted again by
948 centrifugation, PBS was removed, and resuspended with a crRNP complex. The
949 resuspended cells were immediately transferred into the cuvette of the P3 Primary Cell
950 Nucleofector Kit (Lonza; V4SP-3096) and electroporated using code EH-100 on the
951 Lonza 4D-Nucleofector. 80 μL of prewarmed supplemented RPMI media with IL-2, IL-7,
952 and IL-15 was added and cells were allowed to recover for 10 min in the 37°C
953 incubator. 300 μL of fresh media was added and cells are transferred to a 96-well plate.
954 200 μL of additional supplemented media was added 2 days later. The knockout cells
955 are maintained at 1E6 cells/mL with fresh media supplemented with IL-2, IL-7, and IL-
956 15. At 14 days post infection, cells are co-cultured with H80 feeder cells and maintained
957 at 2E6 cells/mL in media supplemented with 20 U/mL IL-2. If AZD5582 treatment
958 applies, cells are treated 1 uM AZD5582 media for 24 hours. At 19 days post infection,
959 cells were stained with Thy1.2 antibody (Biolegend; 140323), fixed with 4% PFA, and
960 underwent flow cytometry analysis (CD FACS Celesta – Fred Hutch Flow Cytometry
961 shared resource).
962
963 **Automated CUT&Tag Profiling**
964 We prepared nuclei from J-Lat 10.6 cells under four conditions: (i) NTC knockout with a
965 treatment of DMSO (negative control) (ii) NTC knockout with a treatment of 10 nM
966 AZD5582 (iii) ING3 knockout with a treatment of DMSO (iv) ING3 knockout with a
967 treatment of 10 nM AZD5582. Up to 10 million cells were pelleted in 1.5 mL microfuge
968 tubes spun at 300 x g for 10 min. Cells were then resuspended in 1 mL of ice cold NE1
969 Buffer (20 mM HEPES-KOH pH 7.9, 10 mM KCl, 0.5 mM Spermidine, 0.1% TritonX-
970 100, 20% Glycerol, with Roche complete EDTA-free protease inhibitor tablet), and
971 incubated on ice for 10 min. Nuclei were then centrifuged at 4°C at 1,300 x g for 4 min.
972 Nuclei were then resuspended in 1 mL of Wash Buffer (20 mM HEPES pH7.5, 150 mM
973 NaCl, 0.5 mM spermidine, supplemented with Roche complete EDTA-free protease
974 inhibitor tablet). 10 μL was used to determine the concentration of native J-Lat 10.6
975 nuclei, and nuclei were diluted to a concentration of 1 million nuclei/900 μL of Wash
976 Buffer and 900 μL aliquots of this suspension was mixed with 100 μL of DMSO in
977 Cryovials, which were then sealed and placed inside a Mr. Frosty isopropanol chamber
978 for slow freezing at -80°C. Nuclei were then stored at -80°C until use. For automated
979 CUT&Tag processing, nuclei were thawed at room temperature, washed in wash buffer,
980 and bound to concanvalin-A (ConA) paramagnetic beads (Bangs Laboratories; BP531)
981 for magnetic separation as described on the protocols.io website

982 (https://doi.org/10.17504/protocols.io.bgztjx6n).Samples were then suspended in
983 antibody binding buffer and split for overnight incubation with antibodies specific to
984 panH4Ac (Active Motif; 39925), BRD4 (Cell Signaling; 13440), RNA-Pol2-S5p (Cell
985 Signaling; 13523), RNA-Pol2-S2p (Cell Signaling; 13499), and IgG control(Abcam;
986 172730). Sample processing was performed in a 96 well plate using 100K Con-A bound
987 nuclei per reaction on a Beckman Coulter Biomek liquid handling robot according to the
988 AutoCUT&Tag protocol available from the protocols.io website
989 (https://doi.org/10.17504/protocols.io.bgztjx6n) and described previously [31] (Fred
990 Hutch Genomics shared resource).
991
992 **CUT&Tag Sequencing Data Processing and Analysis**
993 For AutoCUT&Tag sample pooling and sequencing, the size distribution and molar
994 concentration of libraries were determined using an Agilent 4200 TapeStation, and up to
995 96 barcoded CUT&Tag libraries were pooled at approximately equimolar concentration
996 for sequencing. Paired-end 2 × 50 bp sequencing was performed on the NextSeq 2000
997 platform by the Fred Hutchinson Cancer Research Center Genomics Shared
998 Resources. This yielded 5–10 million reads per antibody. Sequences the extended into
999 the 3' adapter were first removed using the adapter clipping tool by cutadapt 2.9 with
1000 parameters:
1001 -j 8 --nextseq-trim 20 -m 20 -a AGATCGGAAGAGCACACGTCTGAACTCCAGTCA -A
1002 AGATCGGAAGAGCGTCGTGTAGGGAAAGAGTGT -Z.
1003 To construct a reference reflecting integration of HIV-1 into J-Lat cells, we started with
1004 the UCSC hg38 human reference sequence from the Illumina iGenomes collection
1005 (https://support.illumina.com/sequencing/sequencing_software/igenome.html).
1006 Sequence for the integrated HIV-1 genome, including flanking human sequence, was
1007 obtained from accession MN989412.1 [84]. Accounting for flanking human sequence,
1008 we excised chr9:136468439-136468594 from the reference Fasta file and inserted
1009 MN989412.1 in its place. We also rewrote gene & exon annotations downstream of the
1010 integration site, shifting all features in the associated GTF file by 10206bp to account for
1011 newly inserted HIV-1 sequence. Indexes for Bowtie2 v2.4.1 [85] and STAR v2.7.7a [86]
1012 were built using these modified Fasta and GTF files. The HIV-1 insertion is bounded by
1013 a pair of LTRs that, because they comprise identical sequence, are difficult for some
1014 alignment programs to interpret. To avoid these difficulties when needed, another
1015 version of the reference sequence was prepared with the second copy of the LTR
1016 sequence (634bp) masked by 'N's.
1017 Fastq files were aligned to the custom hg38 genome with the HIV-1 genome inserted in
1018 chromosome 9 using Bowtie2 version 2.4.2 with the following parameters: --very-
1019 sensitive-local --soft-clipped-unmapped-tlen --dovetail --no-mixed --no-discordant -q --
1020 phred33 -I 10 -X 1000. Raw sequencing data is available as a GEO DataSet
1021 (GSE215430). Because the read depth and fraction of PCR duplicates varied
1022 considerably between replicates, we removed all duplicate reads from the Bed files.
1023 Peak calling was performed for the BRD4, pan-H4ac, RNA-Pol2-S5p, and RNA-Pol2-
1024 S2p data sets on the pooled reads from all replicates and all conditions using SEACR
1025 version 1.3 [87]. We called peaks using two settings, (1) in which using the IgG control

1026 data with stringent settings, and (2) using a FDR of 0.01, and then used the FDR 0.01
1027 peaks that overlapped with IgG peaks as our final peak set. For correlation analysis
1028 between replicates, the BRD4 peak set was merged with the pan-H4ac peak set, and
1029 the RNA-Pol2-S5p peak set was merged with the RNA-Pol2-S2p peak set. For
1030 statistical comparisons presented in Figure 7, we quantified the base pair coverage of
1031 pan-H4ac or BRD4 over the LTR, the U3 region, or the R + U5 region and these values
1032 were normalized to the total base pair coverage across the genome for each replicate.
1033 Similarly, for comparisons of the RNA-Pol2-S5p data and RNA-Pol2-S2p data, we
1034 quantified the base pair coverage over the LTR, Provirus Body, and Downstream
1035 Region of the HIV provirus these values were normalized to the total base pair coverage
1036 across the genome for each replicate. For comparisons in Figure 7, p-values were
1037 calculated using a two-sample t tests (two sided) with the SciPy.stats.ttest_ind() function
1038 in Python; P values were not corrected for multiple-hypothesis testing. For global
1039 comparison of RNA-Pol2-S5p data between the NTC + DMSO condition and the ING
1040 KO + AZD5582 condition, presented in Figure 8, reads that overlapped RNA-Pol2-S5p
1041 peaks were counted for each replicate and the log 2 Fold Change and adjusted p-
1042 values were calculated using DESeq2 version 1.32.0 using the Wald test. The adjusted
1043 p-values are corrected for multiple-hypothesis testing in a manner that is proportional to
1044 the number of RNA-Pol2-S5p peaks. DESeq2 assigns peaks with extremely sparse
1045 data are assigned an adjusted p-value of NaN, and these peaks were excluded form
1046 downstream analysis.

1047 **References**

1048 1. Deeks, S.G., et al., *HIV infection.* Nat Rev Dis Primers, 2015. **1**: p. 15035.
1049 2. Chun, T.W., et al., *Re-emergence of HIV after stopping therapy.* Nature, 1999. **401**(6756):
1050 p. 874-5.
1051 3. Finzi, D., et al., *Latent infection of CD4+ T cells provides a mechanism for lifelong*
1052 *persistence of HIV-1, even in patients on effective combination therapy.* Nat Med, 1999.
1053 **5**(5): p. 512-7.
1054 4. Sengupta, S. and R.F. Siliciano, *Targeting the Latent Reservoir for HIV-1.* Immunity, 2018.
1055 **48**(5): p. 872-895.
1056 5. Einkauf, K.B., et al., *Intact HIV-1 proviruses accumulate at distinct chromosomal*
1057 *positions during prolonged antiretroviral therapy.* J Clin Invest, 2019. **129**(3): p. 988-998.
1058 6. Jiang, C., et al., *Distinct viral reservoirs in individuals with spontaneous control of HIV-1.*
1059 Nature, 2020. **585**(7824): p. 261-267.
1060 7. Mbonye, U. and J. Karn, *The Molecular Basis for Human Immunodeficiency Virus*
1061 *Latency.* Annu Rev Virol, 2017. **4**(1): p. 261-285.
1062 8. Turner, A.W., et al., *Evaluation of EED Inhibitors as a Class of PRC2-Targeted Small*
1063 *Molecules for HIV Latency Reversal.* ACS Infect Dis, 2020. **6**(7): p. 1719-1733.
1064 9. Li, Z., et al., *The KAT5-Acetyl-Histone4-Brd4 axis silences HIV-1 transcription and*
1065 *promotes viral latency.* PLoS Pathog, 2018. **14**(4): p. e1007012.
1066 10. Nguyen, K., et al., *Multiple Histone Lysine Methyltransferases Are Required for the*
1067 *Establishment and Maintenance of HIV-1 Latency.* mBio, 2017. **8**(1).
1068 11. Nixon, C.C., et al., *Systemic HIV and SIV latency reversal via non-canonical NF-kappaB*
1069 *signalling in vivo.* Nature, 2020. **578**(7793): p. 160-165.
1070 12. Margolis, D.M., et al., *Curing HIV: Seeking to Target and Clear Persistent Infection.* Cell,
1071 2020. **181**(1): p. 189-206.
1072 13. Turner, A.W. and D.M. Margolis, *Chromatin Regulation and the Histone Code in HIV*
1073 *Latency.* Yale J Biol Med, 2017. **90**(2): p. 229-243.
1074 14. Boehm, D. and M. Ott, *Host Methyltransferases and Demethylases: Potential New*
1075 *Epigenetic Targets for HIV Cure Strategies and Beyond.* AIDS Res Hum Retroviruses,
1076 2017. **33**(S1): p. S8-s22.
1077 15. Li, Z., et al., *The BET bromodomain inhibitor JQ1 activates HIV latency through*
1078 *antagonizing Brd4 inhibition of Tat-transactivation.* Nucleic Acids Res, 2013. **41**(1): p.
1079 277-87.
1080 16. Bisgrove, D.A., et al., *Conserved P-TEFb-interacting domain of BRD4 inhibits HIV*
1081 *transcription.* Proc Natl Acad Sci U S A, 2007. **104**(34): p. 13690-5.
1082 17. Conrad, R.J., et al., *The Short Isoform of BRD4 Promotes HIV-1 Latency by Engaging*
1083 *Repressive SWI/SNF Chromatin-Remodeling Complexes.* Mol Cell, 2017. **67**(6): p. 1001-
1084 1012.e6.
1085 18. Friedman, J., et al., *Epigenetic silencing of HIV-1 by the histone H3 lysine 27*
1086 *methyltransferase enhancer of Zeste 2.* J Virol, 2011. **85**(17): p. 9078-89.
1087 19. Tripathy, M.K., et al., *H3K27 Demethylation at the Proviral Promoter Sensitizes Latent*
1088 *HIV to the Effects of Vorinostat in Ex Vivo Cultures of Resting CD4+ T Cells.* J Virol, 2015.
1089 **89**(16): p. 8392-405.

1090 20. Besnard, E., et al., *The mTOR Complex Controls HIV Latency.* Cell Host Microbe, 2016.
1091 **20**(6): p. 785-797.
1092 21. Das, B., et al., *Estrogen receptor-1 is a key regulator of HIV-1 latency that imparts*
1093 *gender-specific restrictions on the latent reservoir.* Proc Natl Acad Sci U S A, 2018.
1094 **115**(33): p. E7795-e7804.
1095 22. Boehm, D., et al., *SMYD2-Mediated Histone Methylation Contributes to HIV-1 Latency.*
1096 Cell Host Microbe, 2017. **21**(5): p. 569-579.e6.
1097 23. Li, Z., et al., *Reiterative Enrichment and Authentication of CRISPRi Targets (REACT)*
1098 *identifies the proteasome as a key contributor to HIV-1 latency.* PLoS Pathog, 2019.
1099 **15**(1): p. e1007498.
1100 24. Huang, H., et al., *A CRISPR/Cas9 screen identifies the histone demethylase MINA53 as a*
1101 *novel HIV-1 latency-promoting gene (LPG).* Nucleic Acids Res, 2019. **47**(14): p. 7333-
1102 7347.
1103 25. Rathore, A., et al., *CRISPR-based gene knockout screens reveal deubiquitinases involved*
1104 *in HIV-1 latency in two Jurkat cell models.* Sci Rep, 2020. **10**(1): p. 5350.
1105 26. Pedersen, S.F., et al., *Inhibition of a Chromatin and Transcription Modulator, SLTM,*
1106 *Increases HIV-1 Reactivation Identified by a CRISPR Inhibition Screen.* J Virol, 2022: p.
1107 e0057722.
1108 27. Pache, L., et al., *BIRC2/cIAP1 Is a Negative Regulator of HIV-1 Transcription and Can Be*
1109 *Targeted by Smac Mimetics to Promote Reversal of Viral Latency.* Cell Host Microbe,
1110 2015. **18**(3): p. 345-53.
1111 28. Jordan, A.B., D.; Verdin, E., *HIV reproducibly establishes a latent infection after acute*
1112 *infection of T cells in vitro.* The EMBO Journal, 2003. **22**: p. 1868-1877.
1113 29. Chan, J.K., et al., *Calcium/calcineurin synergizes with prostratin to promote NF-kappaB*
1114 *dependent activation of latent HIV.* PLoS One, 2013. **8**(10): p. e77749.
1115 30. OhAinle, M., et al., *A virus-packageable CRISPR screen identifies host factors mediating*
1116 *interferon inhibition of HIV.* Elife, 2018. **7**.
1117 31. Janssens, D.H., et al., *Automated CUT&Tag profiling of chromatin heterogeneity in*
1118 *mixed-lineage leukemia.* Nat Genet, 2021. **53**(11): p. 1586-1596.
1119 32. Medvedeva, Y.A., et al., *EpiFactors: a comprehensive database of human epigenetic*
1120 *factors and complexes.* Database, 2015. **2015**.
1121 33. Sanjana, N.E., O. Shalem, and F. Zhang, *Improved vectors and genome-wide libraries for*
1122 *CRISPR screening.* Nat Methods, 2014. **11**(8): p. 783-784.
1123 34. Spina, C.A., et al., *An in-depth comparison of latent HIV-1 reactivation in multiple cell*
1124 *model systems and resting CD4+ T cells from aviremic patients.* PLoS Pathog, 2013.
1125 **9**(12): p. e1003834.
1126 35. Li, W., et al., *MAGeCK enables robust identification of essential genes from genome-*
1127 *scale CRISPR/Cas9 knockout screens.* Genome Biology, 2014. **15**(12): p. 554.
1128 36. Yang, Z., et al., *Recruitment of P-TEFb for stimulation of transcriptional elongation by the*
1129 *bromodomain protein Brd4.* Mol Cell, 2005. **19**(4): p. 535-45.
1130 37. Doyon, Y., et al., *Structural and functional conservation of the NuA4 histone*
1131 *acetyltransferase complex from yeast to humans.* Mol Cell Biol, 2004. **24**(5): p. 1884-96.

1132 38. Ginsburg, D.S., C.K. Govind, and A.G. Hinnebusch, *NuA4 lysine acetyltransferase Esa1 is*
1133 *targeted to coding regions and stimulates transcription elongation with Gcn5.* Mol Cell
1134 Biol, 2009. **29**(24): p. 6473-87.
1135 39. Doyon, Y. and J. Côté, *The highly conserved and multifunctional NuA4 HAT complex.* Curr
1136 Opin Genet Dev, 2004. **14**(2): p. 147-54.
1137 40. Ruhl, D.D., et al., *Purification of a human SRCAP complex that remodels chromatin by*
1138 *incorporating the histone variant H2A.Z into nucleosomes.* Biochemistry, 2006. **45**(17): p.
1139 5671-7.
1140 41. Mizuguchi, G., et al., *ATP-driven exchange of histone H2AZ variant catalyzed by SWR1*
1141 *chromatin remodeling complex.* Science, 2004. **303**(5656): p. 343-8.
1142 42. Luk, E., et al., *Stepwise histone replacement by SWR1 requires dual activation with*
1143 *histone H2A.Z and canonical nucleosome.* Cell, 2010. **143**(5): p. 725-36.
1144 43. Zhou, Y., et al., *Metascape provides a biologist-oriented resource for the analysis of*
1145 *systems-level datasets.* Nat Commun, 2019. **10**(1): p. 1523.
1146 44. Hsiau, T., et al., *Inference of CRISPR Edits from Sanger Trace Data.* bioRxiv, 2019: p.
1147 251082.
1148 45. Hiatt, J., et al., *A functional map of HIV-host interactions in primary human T cells.* Nat
1149 Commun, 2022. **13**(1): p. 1752.
1150 46. Rountree, M.R., K.E. Bachman, and S.B. Baylin, *DNMT1 binds HDAC2 and a new co-*
1151 *repressor, DMAP1, to form a complex at replication foci.* Nat Genet, 2000. **25**(3): p. 269-
1152 77.
1153 47. Pintard, L., A. Willems, and M. Peter, *Cullin-based ubiquitin ligases: Cul3-BTB complexes*
1154 *join the family.* Embo j, 2004. **23**(8): p. 1681-7.
1155 48. Jefferys, S.R., et al., *Epigenomic characterization of latent HIV infection identifies latency*
1156 *regulating transcription factors.* PLoS Pathog, 2021. **17**(2): p. e1009346.
1157 49. Yang, H.C., et al., *Small-molecule screening using a human primary cell model of HIV*
1158 *latency identifies compounds that reverse latency without cellular activation.* J Clin
1159 Invest, 2009. **119**(11): p. 3473-86.
1160 50. Peterson, J.J., et al., *A histone deacetylase network regulates epigenetic reprogramming*
1161 *and viral silencing in HIV infected cells.* bioRxiv, 2022: p. 2022.05.09.491199.
1162 51. Chu, V.T., et al., *Increasing the efficiency of homology-directed repair for CRISPR-Cas9-*
1163 *induced precise gene editing in mammalian cells.* Nat Biotechnol, 2015. **33**(5): p. 543-8.
1164 52. Langer, S., et al., *The E3 Ubiquitin-Protein Ligase Cullin 3 Regulates HIV-1 Transcription.*
1165 Cells, 2020. **9**(9).
1166 53. Doyon, Y., et al., *ING tumor suppressor proteins are critical regulators of chromatin*
1167 *acetylation required for genome expression and perpetuation.* Mol Cell, 2006. **21**(1): p.
1168 51-64.
1169 54. Hsin, J.P. and J.L. Manley, *The RNA polymerase II CTD coordinates transcription and RNA*
1170 *processing.* Genes Dev, 2012. **26**(19): p. 2119-37.
1171 55. Czudnochowski, N., C.A. Bösken, and M. Geyer, *Serine-7 but not serine-5*
1172 *phosphorylation primes RNA polymerase II CTD for P-TEFb recognition.* Nat Commun,
1173 2012. **3**: p. 842.

1174 56. Ravens, S., et al., *Tip60 complex binds to active Pol II promoters and a subset of*
1175 *enhancers and co-regulates the c-Myc network in mouse embryonic stem cells.*
1176 Epigenetics Chromatin, 2015. **8**: p. 45.
1177 57. Devoucoux, M., et al., *Oncogenic ZMYND11-MBTD1 fusion protein anchors the*
1178 *NuA4/TIP60 histone acetyltransferase complex to the coding region of active genes.* Cell
1179 Rep, 2022. **39**(11): p. 110947.
1180 58. Li, J., et al., *ZMYND11-MBTD1 induces leukemogenesis through hijacking NuA4/TIP60*
1181 *acetyltransferase complex and a PWWP-mediated chromatin association mechanism.*
1182 Nat Commun, 2021. **12**(1): p. 1045.
1183 59. Auger, A., et al., *Eaf1 is the platform for NuA4 molecular assembly that evolutionarily*
1184 *links chromatin acetylation to ATP-dependent exchange of histone H2A variants.* Mol
1185 Cell Biol, 2008. **28**(7): p. 2257-70.
1186 60. Dey, A., et al., *The double bromodomain protein Brd4 binds to acetylated chromatin*
1187 *during interphase and mitosis.* Proc Natl Acad Sci U S A, 2003. **100**(15): p. 8758-63.
1188 61. Dey, A., et al., *A bromodomain protein, MCAP, associates with mitotic chromosomes and*
1189 *affects G(2)-to-M transition.* Mol Cell Biol, 2000. **20**(17): p. 6537-49.
1190 62. Kanno, T., et al., *Selective recognition of acetylated histones by bromodomain proteins*
1191 *visualized in living cells.* Mol Cell, 2004. **13**(1): p. 33-43.
1192 63. Jang, M.K., et al., *The bromodomain protein Brd4 is a positive regulatory component of*
1193 *P-TEFb and stimulates RNA polymerase II-dependent transcription.* Mol Cell, 2005. **19**(4):
1194 p. 523-34.
1195 64. Ott, M., et al., *Acetylation of the HIV-1 Tat protein by p300 is important for its*
1196 *transcriptional activity.* Curr Biol, 1999. **9**(24): p. 1489-92.
1197 65. Lusic, M., et al., *Regulation of HIV-1 gene expression by histone acetylation and factor*
1198 *recruitment at the LTR promoter.* Embo j, 2003. **22**(24): p. 6550-61.
1199 66. Van Lint, C., et al., *Transcriptional activation and chromatin remodeling of the HIV-1*
1200 *promoter in response to histone acetylation.* Embo j, 1996. **15**(5): p. 1112-20.
1201 67. Benkirane, M., et al., *Activation of integrated provirus requires histone*
1202 *acetyltransferase. p300 and P/CAF are coactivators for HIV-1 Tat.* J Biol Chem, 1998.
1203 **273**(38): p. 24898-905.
1204 68. Hottiger, M.O. and G.J. Nabel, *Interaction of human immunodeficiency virus type 1 Tat*
1205 *with the transcriptional coactivators p300 and CREB binding protein.* J Virol, 1998.
1206 **72**(10): p. 8252-6.
1207 69. Marzio, G., et al., *HIV-1 tat transactivator recruits p300 and CREB-binding protein*
1208 *histone acetyltransferases to the viral promoter.* Proc Natl Acad Sci U S A, 1998. **95**(23):
1209 p. 13519-24.
1210 70. Col, E., et al., *The histone acetyltransferase, hGCN5, interacts with and acetylates the*
1211 *HIV transactivator, Tat.* J Biol Chem, 2001. **276**(30): p. 28179-84.
1212 71. Steger, D.J., et al., *Purified histone acetyltransferase complexes stimulate HIV-1*
1213 *transcription from preassembled nucleosomal arrays.* Proc Natl Acad Sci U S A, 1998.
1214 **95**(22): p. 12924-9.
1215 72. Winter, G.E., et al., *BET Bromodomain Proteins Function as Master Transcription*
1216 *Elongation Factors Independent of CDK9 Recruitment.* Mol Cell, 2017. **67**(1): p. 5-18.e19.

1217 73. Falcinelli, S.D., et al., *Combined noncanonical NF-κB agonism and targeted BET*
1218 *bromodomain inhibition reverse HIV latency ex vivo.* J Clin Invest, 2022. **132**(8).
1219 74. Schröder, A.R., et al., *HIV-1 integration in the human genome favors active genes and*
1220 *local hotspots.* Cell, 2002. **110**(4): p. 521-9.
1221 75. Almeida, M., et al., *PCGF3/5-PRC1 initiates Polycomb recruitment in X chromosome*
1222 *inactivation.* Science, 2017. **356**(6342): p. 1081-1084.
1223 76. Sharma, A.L., et al., *CBF-1 Promotes the Establishment and Maintenance of HIV Latency*
1224 *by Recruiting Polycomb Repressive Complexes, PRC1 and PRC2, at HIV LTR.* Viruses,
1225 2020. **12**(9).
1226 77. Gonçalves, E., et al., *Minimal genome-wide human CRISPR-Cas9 library.* Genome Biol,
1227 2021. **22**(1): p. 40.
1228 78. Dai, W., et al., *Genome-wide CRISPR screens identify combinations of candidate latency*
1229 *reversing agents for targeting the latent HIV-1 reservoir.* Sci Transl Med, 2022. **14**(667):
1230 p. eabh3351.
1231 79. Humbert, O., et al., *Development of Third-generation Cocal Envelope Producer Cell Lines*
1232 *for Robust Lentiviral Gene Transfer into Hematopoietic Stem Cells and T-cells.* Mol Ther,
1233 2016. **24**(7): p. 1237-46.
1234 80. Meier, J.A., F. Zhang, and N.E. Sanjana, *GUIDES: sgRNA design for loss-of-function*
1235 *screens.* Nat Methods, 2017. **14**(9): p. 831-832.
1236 81. Langmead, B., et al., *Ultrafast and memory-efficient alignment of short DNA sequences*
1237 *to the human genome.* Genome Biol, 2009. **10**(3): p. R25.
1238 82. Roesch, F., M. OhAinle, and M. Emerman, *A CRISPR screen for factors regulating*
1239 *SAMHD1 degradation identifies IFITMs as potent inhibitors of lentiviral particle delivery.*
1240 Retrovirology, 2018. **15**(1): p. 26.
1241 83. Vermeire, J., et al., *Quantification of reverse transcriptase activity by real-time PCR as a*
1242 *fast and accurate method for titration of HIV, lenti- and retroviral vectors.* PLoS One,
1243 2012. **7**(12): p. e50859.
1244 84. Chung, C.H., et al., *Integrated Human Immunodeficiency Virus Type 1 Sequence in J-Lat*
1245 *10.6.* Microbiol Resour Announc, 2020. **9**(18).
1246 85. Langmead, B. and S.L. Salzberg, *Fast gapped-read alignment with Bowtie 2.* Nat
1247 Methods, 2012. **9**(4): p. 357-9.
1248 86. Dobin, A., et al., *STAR: ultrafast universal RNA-seq aligner.* Bioinformatics, 2013. **29**(1):
1249 p. 15-21.
1250 87. Meers, M.P., D. Tenenbaum, and S. Henikoff, *Peak calling by Sparse Enrichment Analysis*
1251 *for CUT&RUN chromatin profiling.* Epigenetics Chromatin, 2019. **12**(1): p. 42.
1252

1253

Figure 1

A

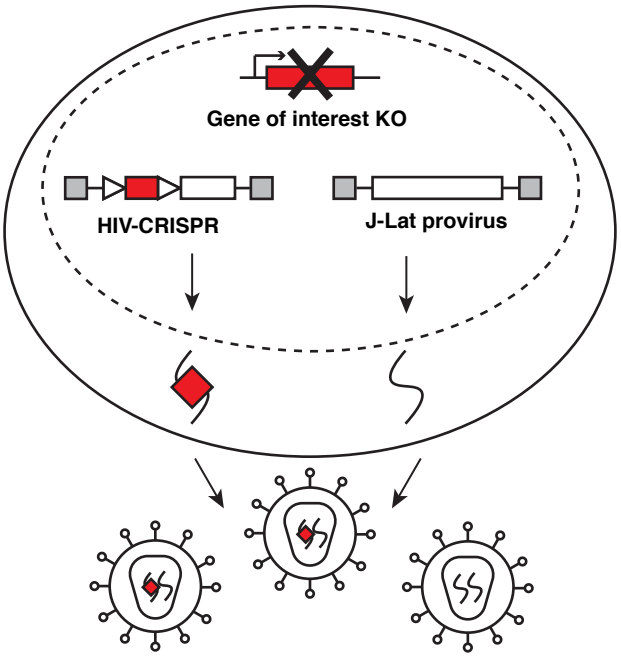

D

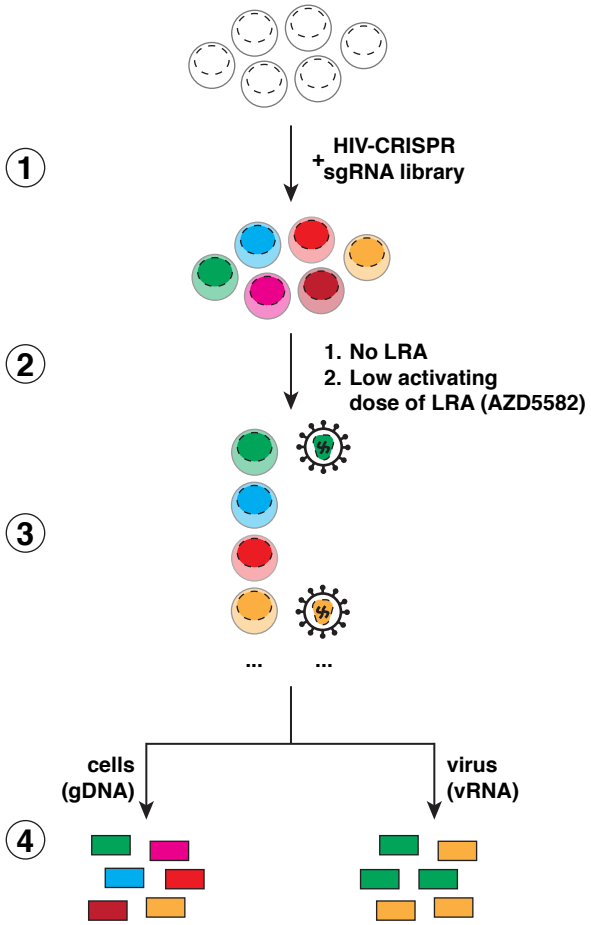

B

	Number of Genes
Histones	84
Histone binders	128
Histone modifiers	365
General chromatin associated	221
Other	43

C

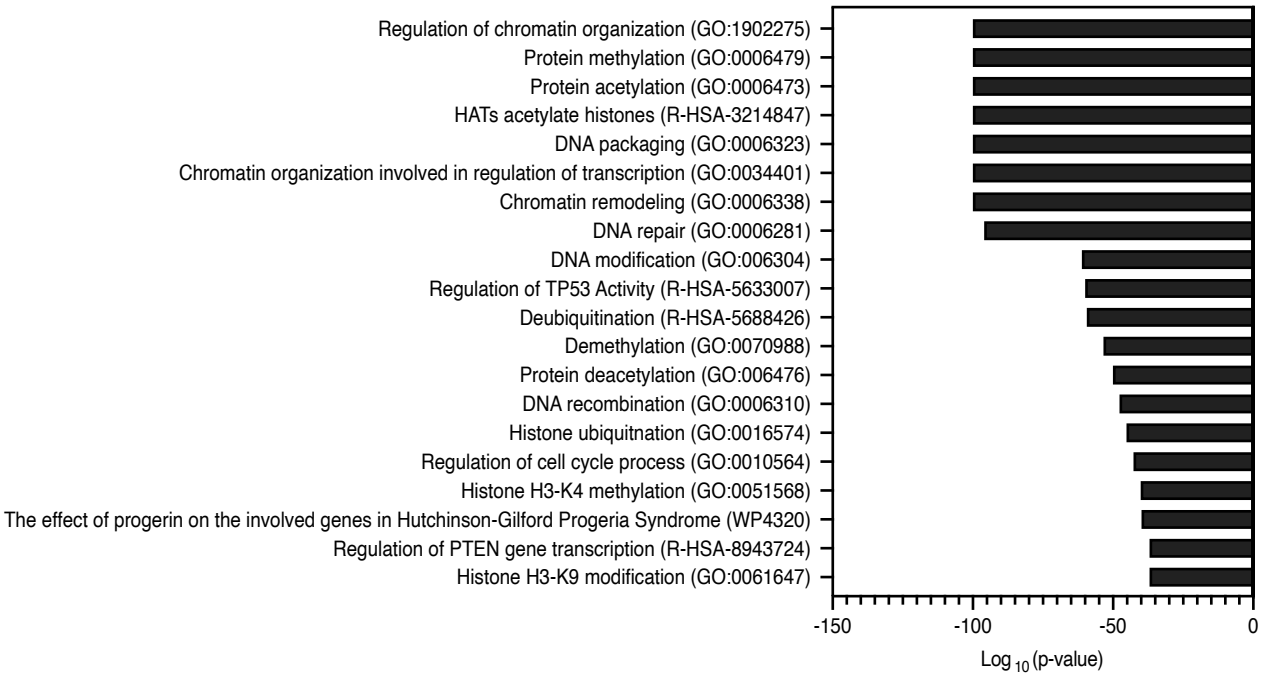

Figure 2

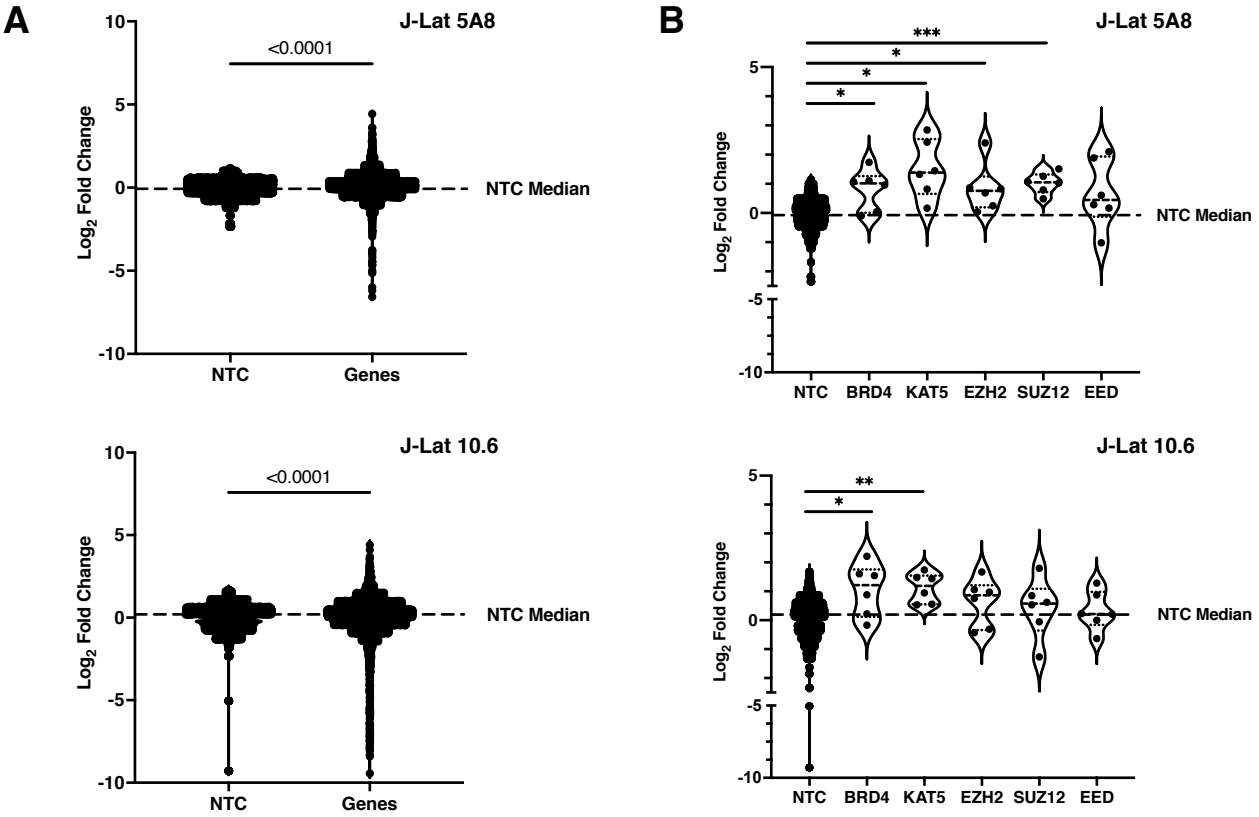
A
J-Lat 5A8
<0.0001
Log2 Fold Change
NTC Median
NTC
Genes
J-Lat 10.6
<0.0001
Log2 Fold Change
NTC Median
NTC
Genes
B
J-Lat 5A8
***
*
*
*
Log2 Fold Change
NTC Median
NTC
BRD4
KAT5
EZH2
SUZ12
EED
J-Lat 10.6
**
*
Log2 Fold Change
NTC Median
NTC
BRD4
KAT5
EZH2
SUZ12
EED

Figure 3

A

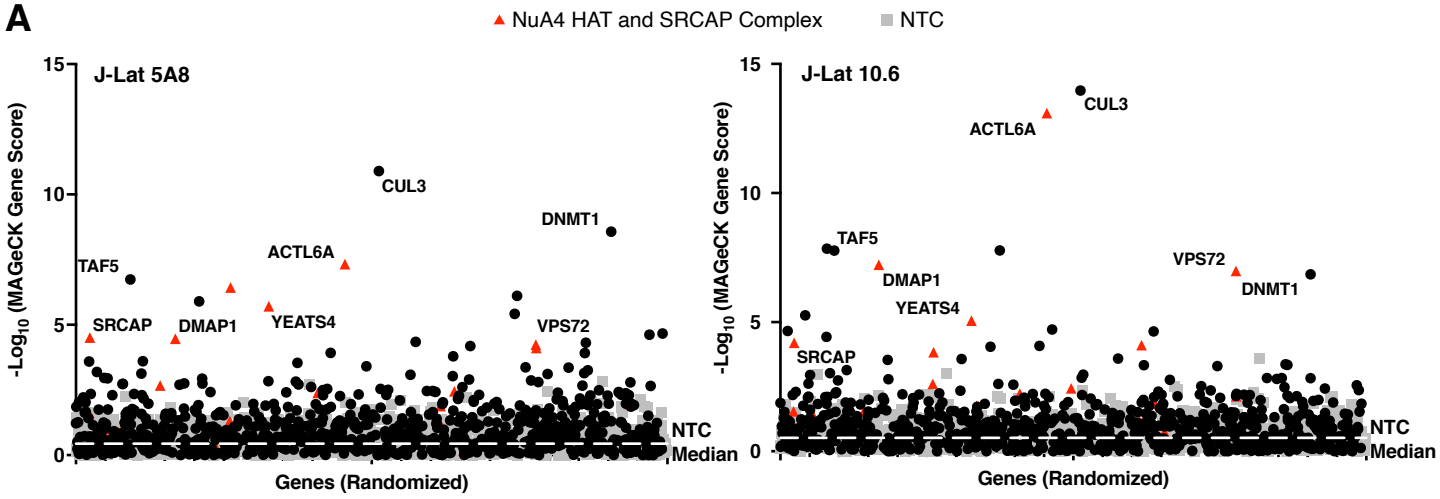

B

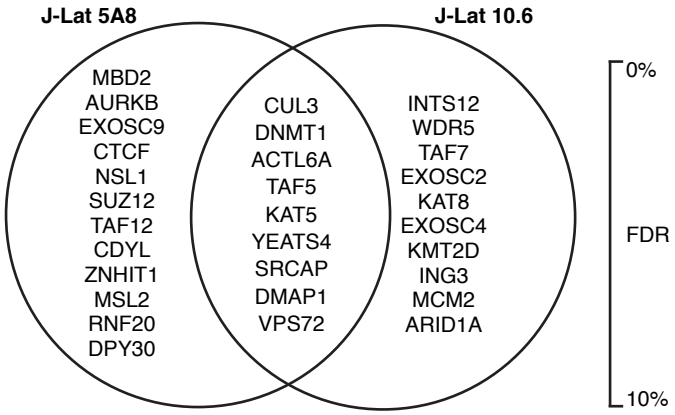

C

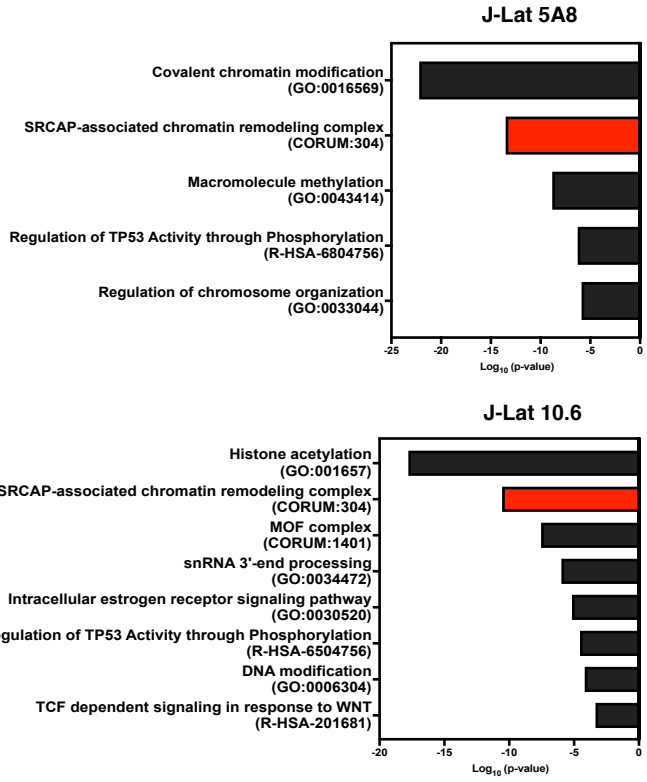

D

		-log$_{10}$ (MAGeCK Gene Score) J-Lat 5A8	J-Lat 10.6
NuA4 HAT complex	TRRAP	2.45	1.85
	EP400	2.38	2.24
	EPC2	0.99	1.33
	EPC1	0.38	0.47
	KAT5	6.43	3.83
	ING3	1.88	4.11
	MRGBP	0.88	0.26
	ACTB	0.19	0.75
	MORF4L1	1.30	2.61
	MORF4L2	1.34	1.18
	MEAF6	2.67	1.54
	MBTD1	1.96	1.17
SRCAP complex	BRD8	1.62	1.54
	DMAP1	4.46	7.22
	RUVBL2	1.25	1.76
	RUVBL1	1.96	0.32
	ACTL6A	7.32	13.10
	VPS72	4.24	6.98
	YEATS4	5.71	5.06
	SRCAP	4.51	4.20
	ACTR6	0.38	2.44
	ZNHIT1	4.11	2.13

Shared

Figure 4

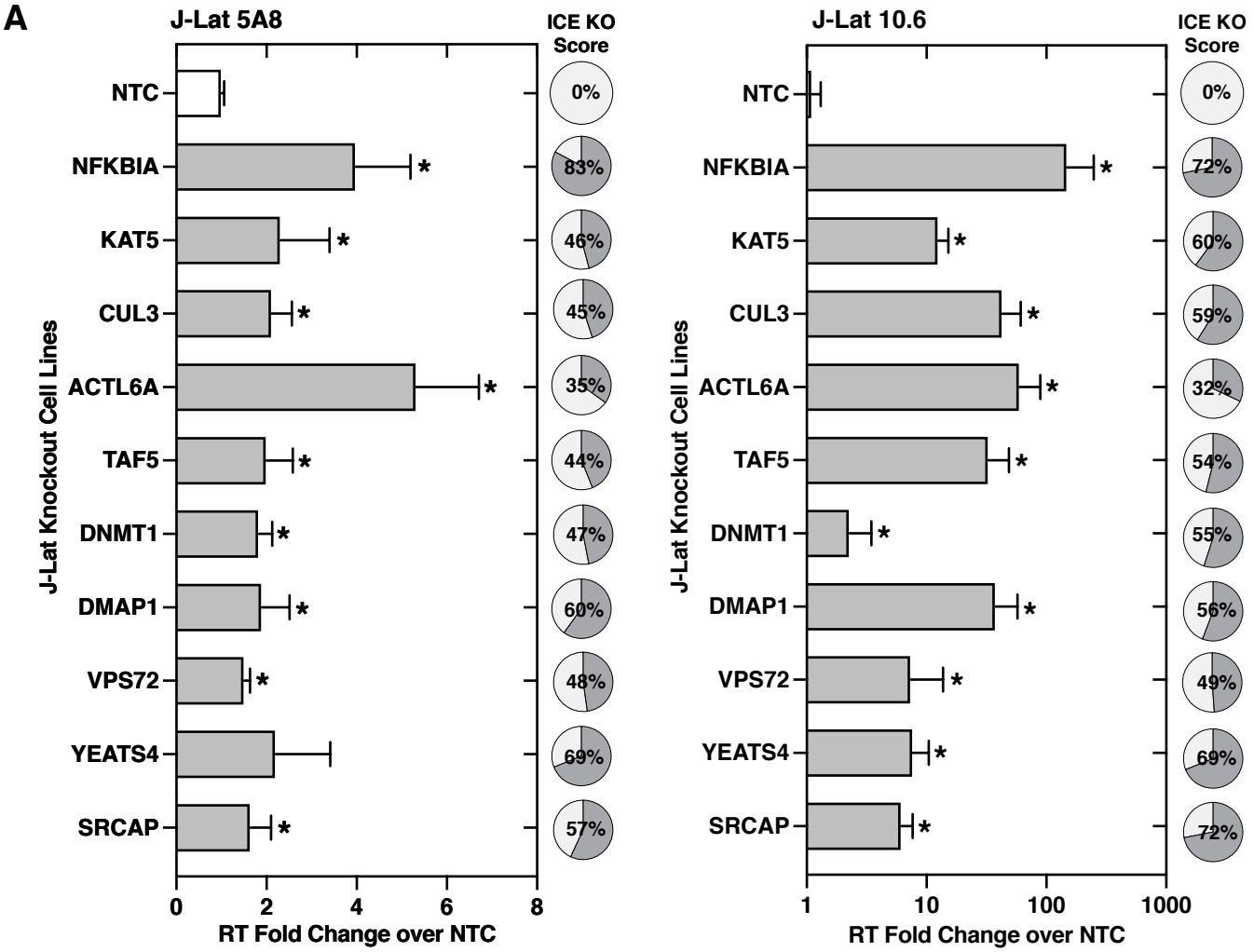
A
J-Lat 5A8
ICE KO Score
NTC
NFKBIA
KAT5
CUL3
ACTL6A
TAF5
DNMT1
DMAP1
VPS72
YEATS4
SRCAP
0%
83%
46%
45%
35%
44%
47%
60%
48%
69%
57%
J-Lat Knockout Cell Lines
0
2
4
6
8
RT Fold Change over NTC
J-Lat 10.6
ICE KO Score
0%
72%
60%
59%
32%
54%
55%
56%
49%
69%
72%
1
10
100
1000
RT Fold Change over NTC

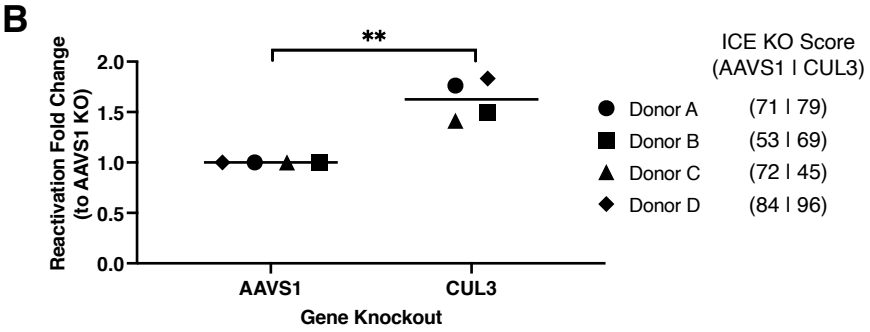
B
**
Reactivation Fold Change (to AAVS1 KO)
2.0
1.5
1.0
0.5
0.0
AAVS1
CUL3
Gene Knockout
ICE KO Score (AAVS1 I CUL3)
Donor A (71 I 79)
Donor B (53 I 69)
Donor C (72 I 45)
Donor D (84 I 96)

Figure 5

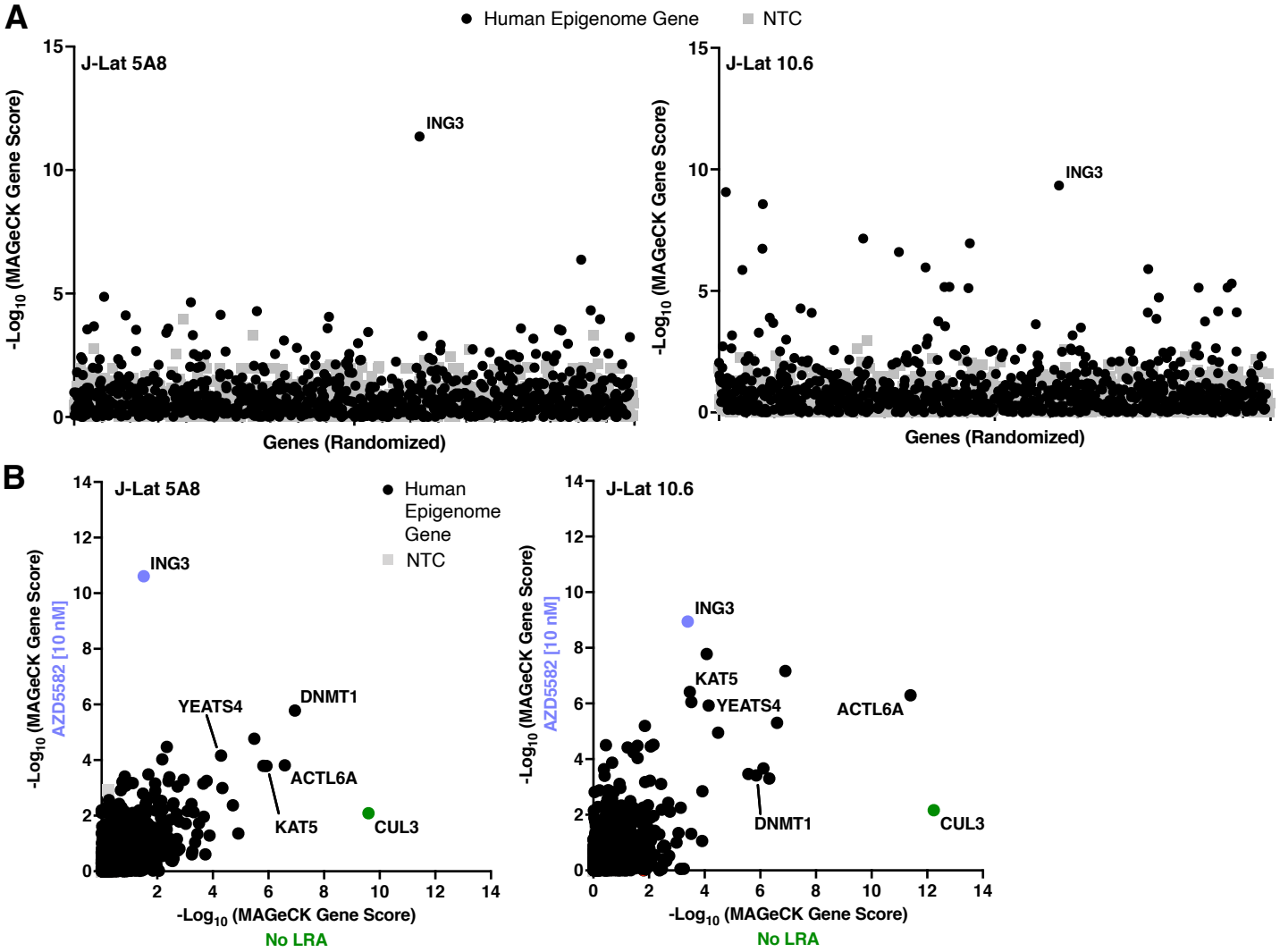
A
Human Epigenome Gene
NTC
J-Lat 5A8
ING3
-Log10 (MAGeCK Gene Score)
Genes (Randomized)
J-Lat 10.6
ING3
-Log10 (MAGeCK Gene Score)
Genes (Randomized)
B
J-Lat 5A8
Human Epigenome Gene
NTC
ING3
YEATS4
DNMT1
ACTL6A
KAT5
CUL3
-Log10 (MAGeCK Gene Score) AZD5582 [10 nM]
-Log10 (MAGeCK Gene Score) No LRA
J-Lat 10.6
ING3
KAT5
YEATS4
ACTL6A
DNMT1
CUL3
-Log10 (MAGeCK Gene Score) AZD5582 [10 nM]
-Log10 (MAGeCK Gene Score) No LRA

Figure 6

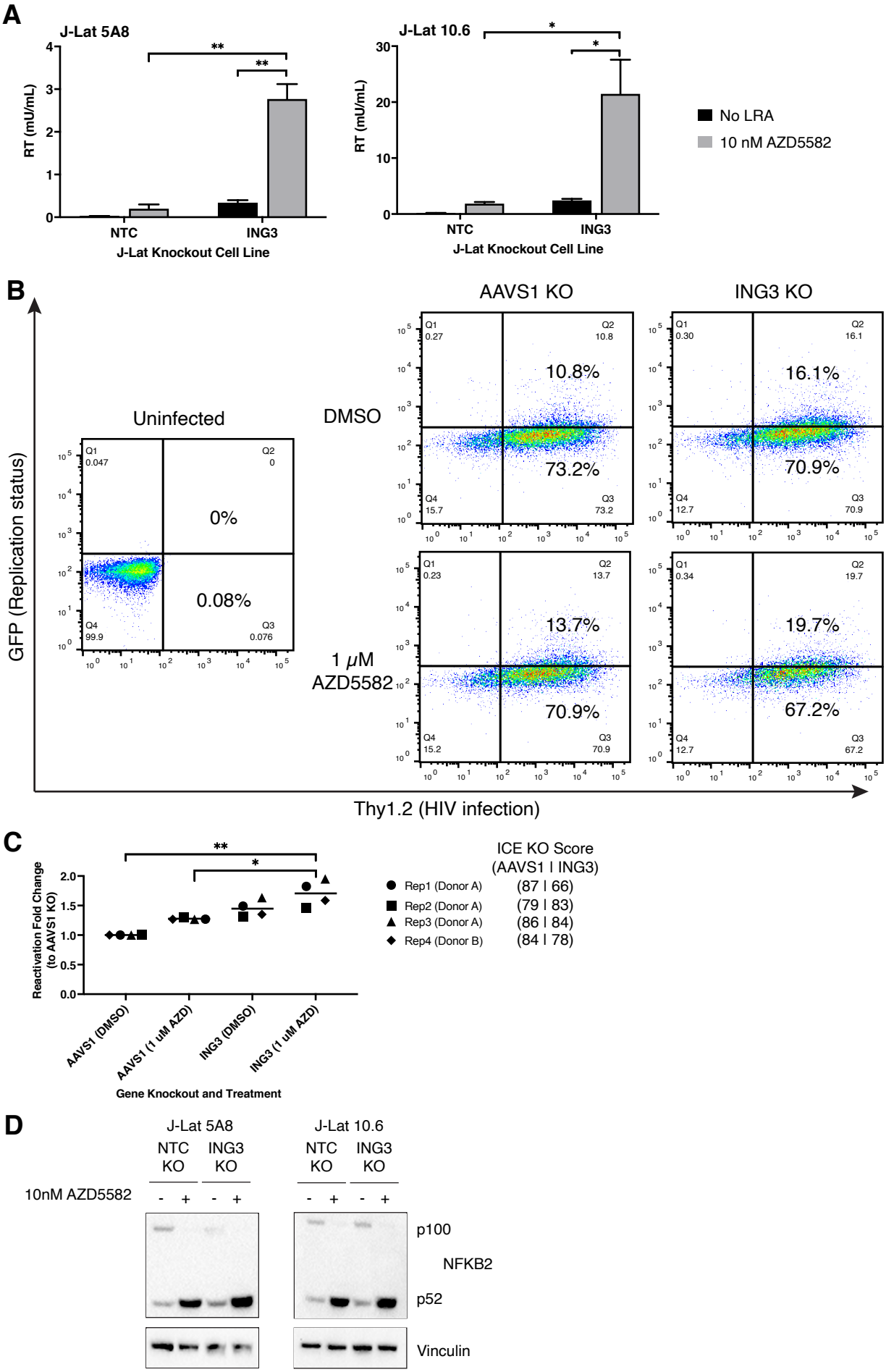
A
J-Lat 5A8
J-Lat 10.6
RT (mU/mL)
NTC
ING3
J-Lat Knockout Cell Line
No LRA
10 nM AZD5582
B
AAVS1 KO
ING3 KO
Uninfected
DMSO
1 μM AZD5582
GFP (Replication status)
Thy1.2 (HIV infection)
0%
0.08%
10.8%
73.2%
16.1%
70.9%
13.7%
70.9%
19.7%
67.2%
C
Reactivation Fold Change (to AAVS1 KO)
AAVS1 (DMSO)
AAVS1 (1 uM AZD)
ING3 (DMSO)
ING3 (1 uM AZD)
Gene Knockout and Treatment
ICE KO Score (AAVS1 | ING3)
Rep1 (Donor A) (87 | 66)
Rep2 (Donor A) (79 | 83)
Rep3 (Donor A) (86 | 84)
Rep4 (Donor B) (84 | 78)
D
J-Lat 5A8
J-Lat 10.6
NTC KO
ING3 KO
10nM AZD5582
p100
NFKB2
p52
Vinculin

Figure 7

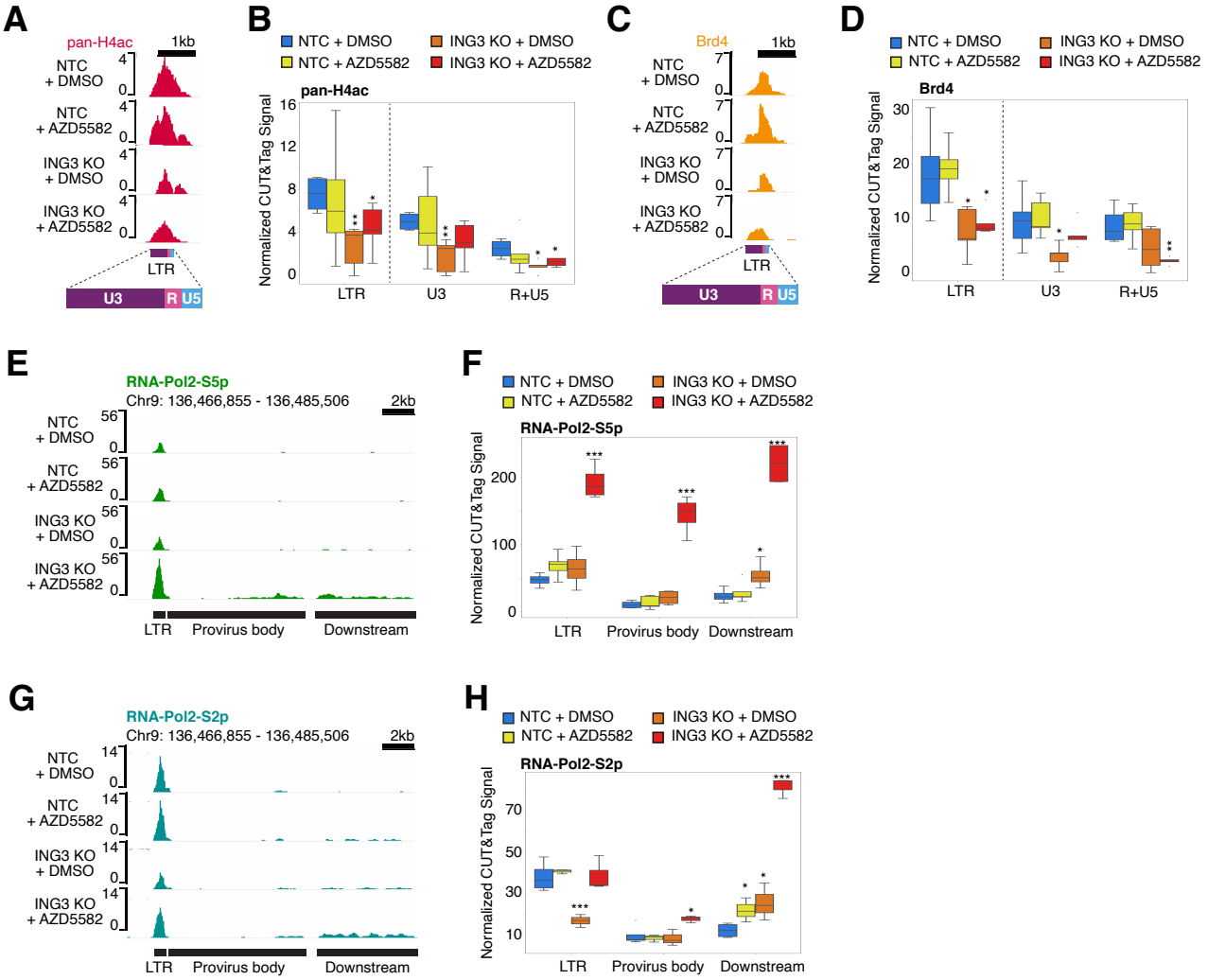
A
pan-H4ac
1kb
NTC + DMSO
NTC + AZD5582
ING3 KO + DMSO
ING3 KO + AZD5582
LTR
U3
R
U5
B
NTC + DMSO
NTC + AZD5582
ING3 KO + DMSO
ING3 KO + AZD5582
pan-H4ac
Normalized CUT&Tag Signal
LTR
U3
R+U5
C
Brd4
1kb
NTC + DMSO
NTC + AZD5582
ING3 KO + DMSO
ING3 KO + AZD5582
LTR
U3
R
U5
D
NTC + DMSO
NTC + AZD5582
ING3 KO + DMSO
ING3 KO + AZD5582
Brd4
Normalized CUT&Tag Signal
LTR
U3
R+U5
E
RNA-Pol2-S5p
Chr9: 136,466,855 - 136,485,506
2kb
NTC + DMSO
NTC + AZD5582
ING3 KO + DMSO
ING3 KO + AZD5582
LTR
Provirus body
Downstream
F
NTC + DMSO
NTC + AZD5582
ING3 KO + DMSO
ING3 KO + AZD5582
RNA-Pol2-S5p
Normalized CUT&Tag Signal
LTR
Provirus body
Downstream
G
RNA-Pol2-S2p
Chr9: 136,466,855 - 136,485,506
2kb
NTC + DMSO
NTC + AZD5582
ING3 KO + DMSO
ING3 KO + AZD5582
LTR
Provirus body
Downstream
H
NTC + DMSO
NTC + AZD5582
ING3 KO + DMSO
ING3 KO + AZD5582
RNA-Pol2-S2p
Normalized CUT&Tag Signal
LTR
Provirus body
Downstream

Figure 8

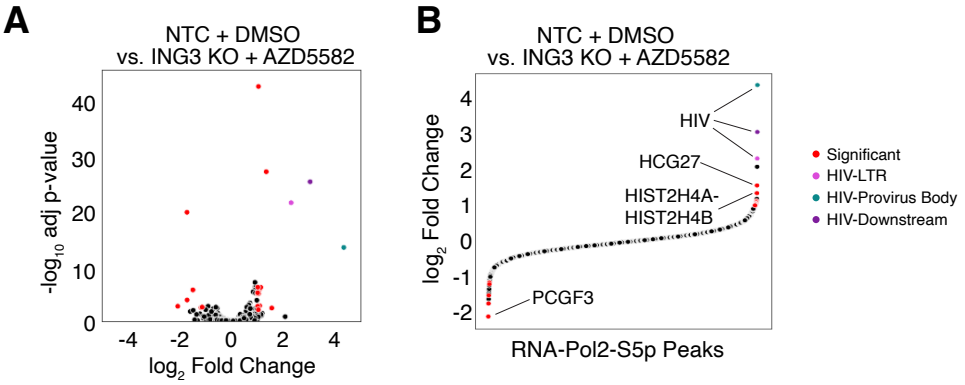
A
NTC + DMSO
vs. ING3 KO + AZD5582
-log10 adj p-value
log2 Fold Change
B
NTC + DMSO
vs. ING3 KO + AZD5582
log2 Fold Change
RNA-Pol2-S5p Peaks
HIV
HCG27
HIST2H4A-
HIST2H4B
PCGF3
Significant
HIV-LTR
HIV-Provirus Body
HIV-Downstream